

Direct Measurements of Upper Ocean Currents and Water Properties Across the Tropical Pacific During the 1990's

GREGORY C. JOHNSON*, BERNADETTE M. SLOYAN¹, WILLIAM S. KESSLER
and KRISTENE E. MCTAGGART
NOAA/Pacific Marine Environmental Laboratory, Seattle, WA 98115-6349, USA

Submitted to *Progress in Oceanography*
May 26, 2001
Revised
October 5, 2001

Abstract

Meridional sections of upper ocean zonal currents, potential temperature, and salinity are estimated at 10 longitudes from 143°E to 95°W using Conductivity-Temperature-Depth and Acoustic Doppler Current Profiler data from 172 synoptic sections taken in the tropical Pacific between 138°E and 86°W, mostly in the 1990's. Data reduction is carried out in a potential isopycnal and mixed layer framework to preserve a sharp pycnocline, a mixed layer, water property extrema, and velocity extrema. Mean zonal currents, potential temperatures, and salinities are produced at each longitude. The seasonal cycles of these fields are also estimated, as well as a simple El Niño Southern Oscillation (ENSO) cycle. Zonal sections along the equator are also presented. Properties of the near-equatorial zonal currents, including transports, temperatures, and salinities, are estimated separately from the synoptic sections. The seasonal cycles of these quantities and their correlations with the Southern Oscillation Index are investigated. The work is distinguished from most existing literature in that direct estimates of zonal velocity are combined with contemporaneous temperature and salinity data, allowing trans-Pacific estimates of near-equatorial current transports and properties, including those of the northern branch of the South Equatorial Current, the New Guinea Coastal Undercurrent, and the Equatorial Undercurrent.

Keywords: Oceanography, Equatorial Circulation, Current Data, Hydrographic data, El Niño Phenomena, Seasonal Variations, Equatorial Pacific Ocean (138°E - 86°W, 8°S - 10°N)

*Corresponding author address: Dr. Gregory C. Johnson, NOAA/Pacific Marine Environmental Laboratory, 7600 Sand Point Way N.E., Bldg. 3, Seattle, WA 98115-6349, U.S.A., Tel: 206-526-6806, Fax: 206-526-6744, E-mail: gjohnson@pmel.noaa.gov

¹Now at: Woods Hole Oceanographic Institution, Woods Hole, MA 02543-1050, USA

1. Introduction

There are many studies of the tropical Pacific Ocean circulation. Only a few of those have sufficient data to describe the mean temperature, salinity, and current field and estimate current transports from contemporaneous observations. The Hawaii-to-Tahiti Shuttle experiment provided a picture of the mean geostrophic currents and water masses in the central tropical Pacific (Wyrtki & Kilonsky, 1984) that is still a standard. This study used Conductivity-Temperature-Depth (CTD) and bottle data taken along 43 meridional sections from 15 cruises between April 1979 and August 1980. The shipboard Acoustic Doppler Current Profiler (ADCP) data from these cruises, while only available over a very limited depth range and with low-quality navigational data by modern standards, also have been thoroughly exploited to examine energy and momentum balances (Johnson & Luther, 1994). In the western Pacific, CTD and ADCP or profiler data (when available) from several observational programs between 1984 and 1991 (27 sections at 165°E and 9 at 142°E) were used in a dynamical interpretation of the local mean circulation (Gouriou & Toole, 1993). Earlier, 21 of these sections had been used to look at the 1986-1987 El Niño and the subsequent La Niña (Delcroix, Eldin, Radenac, Toole & Firing, 1992). In the central and eastern Pacific, meridional CTD/ADCP sections have been used primarily to diagnose horizontal divergence and infer upwelling, with some discussion of the mean zonal currents (Johnson, McPhaden & Firing, 2001). Variations in the salinity maximum and zonal advection in the southern branch of the South Equatorial Current (SEC) have been analyzed using CTD data (Kessler, 1999). The termination of the Equatorial UnderCurrent (EUC) has also been examined with historical hydrographic data in the eastern Pacific (Lukas, 1986). Finally, the structure of the Subsurface CounterCurrents (SCCs) has also recently been examined across the Pacific with meridional CTD/ADCP sections (Rowe, Firing & Johnson, 2000).

Systematic studies of seasonal and interannual variability of tropical Pacific Ocean current transports have been mostly limited to expendable bathythermograph (XBT) data (Donguy & Meyers, 1996; Kessler & Taft, 1987; Taft & Kessler, 1991; Picaut & Tournier, 1991). These studies rely on regional potential temperature–salinity (θ – S) relations and the geostrophic balance. This reliance means that they are usually limited to assuming a zero-velocity surface at 400 m. The wind-driven component of the zonal velocity and other ageostrophic terms are also neglected, although they can be significant near the equator (Bryden & Brady, 1985; Joyce, Lukas & Firing, 1988). In addition, application of geostrophy on the equator is not a trivial exercise. The small meridional density gradients associated with geostrophic zonal velocity on the equator are easily aliased by internal waves and other transients on (Hayes, 1982; Lukas & Firing, 1984; Moum, Chereskin, Park & Regier, 1987; Picaut, Hayes & McPhaden, 1989; Picaut & Tournier, 1991; Cornuelle, Morris & Roemmich, 1993; Lagerloef, Mitchum, Lukas & Niiler, 1999). Thus careful temporal and spatial smoothing is required. Often studies based on XBTs omit current transport estimates near the equator altogether.

In this study upper ocean currents and water-masses are analyzed at 10 longitudes from 143°E to 95°W, spanning most of the zonal extent of the equatorial Pacific. Zonal velocity, potential temperature, and salinity data are presented. The mean fields, as well as their seasonal cycle and linear correlation with the Southern Oscillation Index (SOI, which refers hereafter to the 5-month running mean of normalized monthly values) are estimated.

This work uses 172 synoptic meridional CTD/ADCP sections collected in the tropical Pacific. These data were taken mostly in the 1990's, the majority during the maintenance of the Tropical-Ocean-Atmosphere (TAO) and Triangle Trans-Ocean Buoy Network (TRITON) moorings (Hayes, Mangum, Picaut, Sumi & Takeuchi, 1991; McPhaden et al., 1998).

The paper is structured as follows. The data and their processing are discussed in Section 2. In Section 3 the zonal currents, temperature, and salinity are described. First the means are discussed at all longitudes and along the equator, then the seasonal cycle and the response to the SOI are discussed at western, central, and eastern longitudes as well as along the equator. In Section 4 aspects of the major near-equatorial zonal currents are presented quantitatively through analyses of current transports, positions, and water properties estimated from the synoptic meridional sections. Section 5 concludes the paper.

2. Data and fitting

The 172 synoptic and nominally meridional CTD/ADCP sections used in this study were taken from June 1985 through December 2000 between 138°E and 86°W (Fig. 1). Of these, 103 sections were taken during TAO mooring array maintenance cruises from June 1991 through December 2000 between 165°E and 95°W. The cruises were on the NOAA Ship *Discoverer* in the first half of the decade (e.g., Johnson & Plimpton, 1999) and the NOAA Ships *Ka'imimoana* and *Ronald H. Brown* for the second half of the decade (e.g., McTaggart & Johnson, 1999). Another 29 sections were taken on the R/V *Kaiyo* as part of the Tropical Ocean Climate Study (TOCS, Kashino et al., 2001). The bulk of the remaining sections came from the World Ocean Circulation Experiment (WOCE; Firing, Wijffels & Hacker, 1998) one-time hydrographic survey, the United States/People's Republic of China cooperative program for Air-Sea Interaction (US/PRC; Gouriou & Toole, 1993), the U.S. Joint Global Ocean Flux Study (JGOFS) Equatorial Pacific Process Study (Murray, Johnson & Garside, 1995), the Tropical Ocean Global Atmosphere Coupled Ocean-Atmosphere Response Experiment (TOGA-COARE; Eldin et al., 1994), and the Western Equatorial Pacific Ocean Circulation Study (WEPOCS; Tsuchiya, Lukas, Fine, Firing & Lindstrom, 1989).

The sections were occupied along 10 nominal longitudes (Fig. 1; 143°E, 156°E, 165°E, 180°E, 170°W, 155°W, 140°W, 125°W, 110°W, and 95°W). At each longitude occupations tended to be separated by roughly 6 months or more. Excepting 18 sections occupied from 1985 through 1990 along 165°E as part of US/PRC and WEPOCS, the sections were fairly evenly distributed by year through the 1990's, with as few as 6 in 1991, and as many as 23 in 1997. In longitude the sections were somewhat more concentrated in the western and central Pacific than in the eastern Pacific, with as many as 34 at three closely spaced longitudes around 143°E and 21 at 140°W, and as few as 12 at both 110°W and 95°W. The distribution through the seasonal cycle was biased toward boreal fall. The most uneven 3-month groupings had 61 sections in September–November, 37 sections in December–February, 35 in March–May, and 39 in June–August. The section times also tended slightly to favor El Niño conditions, as did the 1990's. The mean and standard deviation of the SOI at the section times was -0.3 ± 1.0 , the same statistics as for the period of mid-1991 through 2000.

First, the ADCP and CTD data for each individual, quasi-synoptic section are gridded between 8°S and 13°N following Johnson, McPhaden, Rowe & McTaggart (2000). The ADCP generally measures velocity between about 20 m and 300–450 m in 8-m bins, although some earlier measurements extend only to about 200 m. These velocities are

objectively mapped assuming a Gaussian covariance, a meridional correlation length scale of 1° , a vertical correlation length scale of 25 m, and a noise-to-signal energy ratio of 0.01. The objective mapping uses shear in the upper water column to extrapolate velocities to the surface. The CTD temperature, salinity, and pressure data are usually sampled from the surface to at least 1000 dbar at 1-dbar spacing in the vertical and 1° latitude in the horizontal. The station spacing is often 0.5° within $\pm 3^\circ$ of the equator, but occasionally exceeds 1° , mostly in the earlier part of the decade. These fields are gridded somewhat differently from the ADCP data. They are splined in latitude on isopycnals to a regular, closely spaced grid. Both the CTD and the ADCP data are concentrated about the equator (Fig. 1).

Once the individual, quasi-synoptic sections have been gridded, their potential temperature, salinity, and zonal velocity fields are then analyzed around each of the 10 nominal longitudes listed above. For this analysis an isopycnal averaging procedure is applied to potential temperature, salinity, depth, and zonal velocity. This procedure better preserves a sharp pycnocline, water properties, and velocity extrema by reducing the smearing effects of isopycnal heave (Lozier, McCartney & Owens, 1994). By following isopycnals, the averaging is quasi-Lagrangian in the vertical. In contrast to isobaric averaging, this process results in a very sharp thermocline, typical of the strength of a synoptic section. The mixed layer temperature, salinity, and depth as well as zonal velocity are analyzed separately, allowing for vertical shear in the mixed layer zonal velocity. The mixed layer analysis is connected to the permanent pycnocline with a shape-preserving spline (Akima, 1970).

For the averaging, potential temperature, salinity, zonal velocity and depth are independently interpolated onto a closely-spaced latitudinal and isopycnal grid (just latitudinal for the mixed-layer). Data at each latitude and isopycnal from all sections within about 20° of the target longitude are least-squares fitted to a polynomial function of longitude, an annual harmonic, and the SOI. Fitting sections from two or three nominal longitudes means data from more months of the year and in more phases of the SOI are included. At most locations there are data from three nominal longitudes, and the polynomial is second order. However, at the westernmost and easternmost lines at 143°E and 95°W , and anywhere else where only data from two nominal longitudes are available, the polynomial reverts to first order. For the second order cases the fit for the data D looks like $D = a + bx + cx^2 + d\sin(2\pi t/T) + f\cos(2\pi t/T) + gS$, where $a - g$ are the fit coefficients, x is the longitude, t is the time (in years) when the data were taken, T is the period of a year, and S is the value of the SOI interpolated to the time t . Averages are displayed only where greater than 16 sections are locally available for fitting.

3. Zonal velocity, potential temperature, and salinity fields

This data set allows an investigation into the longitudinal, seasonal, and interannual evolution of the mean upper ocean zonal currents and water masses across the equatorial Pacific. The mean zonal velocity sections at the 10 longitudes and along the equator are discussed first and then related to mean sections of potential temperature and salinity. Following this discussion of the means, the seasonal cycle and the linear regression against the SOI (a simple means of evaluating the ENSO cycle) are described at a western longitude, a central longitude, and an eastern longitude, as well as along the equator.

3.1 The mean fields

The mean sections of zonal velocity (Fig. 2), show the two major westward currents (unshaded regions), the SEC, and the Equatorial Intermediate Current (EIC). The surface-intensified SEC is split into a northern and a southern branch (Wyrski, 1974a), here referred to as SEC(N) and SEC(S). At 155°W the SEC(N) is centered at 2°N and the SEC(S) at 3°S. These branches are separated by a near-equatorial minimum in westward surface flow, or at some times eastward surface flow (McPhaden & Taft, 1988). The EIC (Delcroix & Henin, 1988) is most obvious in the western half of the basin. At 155°W it is centered around 1°N, 350 m. In the far western section, at 143°E, the zonal component of the New Guinea Coastal Undercurrent (NGCUC; Tsuchiya et al., 1989; Butt & Lindstrom, 1994), a western boundary current, is centered near 200 m, 2.5°S, just off the coast.

The SEC(N) is strongest in the central Pacific, building in strength from 95°W to 140°W, and then declining to almost nothing by 165°E, and continuing weak to 143°E. Like the SEC(N), the SEC(S) is surface-intensified in the east where the thermocline is shallow, but it deepens considerably by the dateline. The SEC(S) also builds in strength from the eastern to the central Pacific, but maintains its strength further west, weakening by 156°E. Both branches of the SEC have deep extensions in the east, that reach far below the thermocline (Fig. 3). These deep branches are strongest at 110°W, but are visible from 140°W to 95°W.

The EIC is very weak or nonexistent in the east, and in some sections is apparent only as a minimum in eastward velocity around 0°, 350 m. By 155°W a robust EIC is centered near 350 m, 1°N, and it shifts equatorward to the west of that longitude. The current strengthens and deepens from 155°W to 165°E, where it is too deep to be fully sampled by the ADCP measurements, which tend to drop out below 350 m. The deep extension of the SEC(N) in the east may be connected to the EIC in the west.

The NGCUC is only evident at 143°W, as a subsurface velocity maximum in the south of the section. This current is not discussed extensively in other sections since it is not a transpacific current. However, the feature is significant to the general circulation, so some statistics are computed from the mean section. The NGCUC mean zonal volume transport is about $-19 \times 10^6 \text{ m}^3 \text{ s}^{-1}$, with a velocity-weighted potential temperature of 18.85°C, salinity of 35.18, and potential density anomaly of 25.06 kg m^{-3} .

Eastward currents (Fig. 2, shaded regions) include the EUC, the North Equatorial Countercurrent (NECC), and the SCCs. At 140°W the core of the EUC is located near 0°, 110 m and the NECC is a near-surface current centered around 7°N. The SCCs, or Tsuchiya Jets (Tsuchiya, 1975; Johnson & Moore, 1997), are deeper eastward currents, also known as the Northern Subsurface Countercurrent (NSCC) and the two branches of the Southern Subsurface Countercurrent (SSCC). At 140°W the NSCC is centered near 4°N, 200 m and the SSCCs are centered near 4.5°S, 200 m and 7°S, 250 m. In addition, the northern edge of the surface-intensified South Equatorial Countercurrent (SECC) can be seen in some of the sections in the west, for instance, near 8°S at 165°E.

The EUC starts out deep and relatively weak at 143°E, where it is displaced to the north of the equator by the NGCUC (Fig. 2). The EUC builds to 156°E, but appears to weaken at 165°E before building to full strength between 155°W and 125°W, and then weakening considerably by 95°W. The maximum EUC velocity occurs at 125°W. The EUC shoals steadily eastward to 110°W, with its center in the thermocline, near $\theta = 17^\circ\text{C}$ (Fig. 3).

This behavior is in agreement with a velocity climatology from TAO moored current meter and ADCP data (Yu & McPhaden, 1999). Their data are not spatially resolved to show the EUC weakening near 165°E, but similar behavior does occur in models (Fig. 8 of Vintzileos, Delecluse & Sadourny, 1999) and observations suggest a reversal in the zonal pressure gradient at the core of the EUC near these longitudes (Fig. 2 of Johnson et al., 2000). On the other hand the EUC weakening at 165°E could be due to insufficient sampling. Around 140°W, where the trade winds are at their peak, the entire equatorial current system, including the EUC, the SEC(N) and the NECC, is most intense, in qualitative agreement with surface drifter climatological velocities (Reverdin, Frankignoul, Kestenare & McPhaden, 1994; Johnson, 2001).

The NECC shifts north from 4°N at 143°E to 6°N at 165°E and about 8°N by 125°W (Fig. 2). The velocity maximum in the NECC starts out strong at 143°E, weakens to 165°E, builds to 140°W before weakening significantly and moving south at 110°W, then rebuilds and moves back north at 95°W, again consistent with surface velocities from drifters. The pattern in the eastern and central Pacific is expected from the Sverdrup relation (Kessler, 2001). At many latitudes the NECC velocity maximum is slightly subsurface, which is due to a combination of two factors: First, the westward Ekman tendency at the surface from southerly winds. Second, a near-surface geostrophic tendency toward westward flow induced by northward surface warming and freshening across the NECC.

The SCCs also evolve from west to east (Fig. 2). In the west, the SCCs appear as deep lobes on the EUC with velocity maxima approaching 30 cm s^{-1} . The SCCs shift poleward and upward to the east. By 140°W they are fully separated from the EUC. In synoptic sections the SCCs are still strong in the central Pacific (Rowe et al., 2000), but because they are surrounded by westward flow and meander significantly, probably influenced by Tropical Instability Waves (TIWs, Baturin & Niiler, 1997), they are weak in the mean. By 110°W the SSCs are quite shallow and have moved significantly poleward, with the southern SSC south of 8°S, and by 95°W, the NSCC has all but disappeared, likely turning north under the Costa Rica Dome (Johnson & McPhaden, 1999; Kessler, 2001). The NSCC and NECC are sometimes difficult to separate, with only a minimum in eastward velocity found between them.

Finally, a portion of the South Equatorial Countercurrent (SECC; Reid, 1959, 1961; Merle, Rotschi & Voituriez, 1969; Wyrki, 1974a; Eldin, 1983; Kessler & Taft, 1987; Delcroix, Eldin & Henin, 1987) is visible at the southern edge of the sections at 165°E to 170°W in the mean. However, the sampling of this current is insufficient for discussion here.

The shape of the thermocline is related to these currents through the geostrophic balance (Fig. 3). Isotherms slope up toward the equator below the SEC, as the thermocline sharpens approaching $\pm 2^\circ$ latitude. Inside of this range, the thermocline spreads vertically around the zonal velocity maximum of the EUC, as geostrophy requires. There is a poleward thermocline uplift in the northern portion of the sections, geostrophically associated with the NECC, and a slight poleward uplift in the very southern portion of the western sections, associated with the SECC. The sharp subthermocline meridional fronts in temperature, found poleward of the tropical 13°C thermostad, are associated with the SSC and NSCC. The thermostad builds poleward to the east as these currents, which flank it, move poleward under the shoaling thermocline to conserve potential vorticity (Johnson & Moore, 1997). Finally, isotherms pinch equatorward below this thermostad, near 11°C , associated with a relative minimum in eastward flow in the east and the westward flowing EIC in the west.

In the equatorial region the thermocline shoals eastward and thereby provides the zonal pressure gradient on the equator that drives the EUC (Fig. 3). In the western equatorial Pacific the trade winds pile up a thick layer of warm surface water above a deep thermocline, the warm pool (Webster & Lukas, 1992), while in the eastern equatorial Pacific the thermocline rises to the surface, creating the cold tongue (Bryden & Brady, 1985). There is a subtle reversal of isotherm slopes below about 15°C between 156°E and 165°E (and hence in zonal pressure gradient) that is concordant with a reduction in the strength of the EUC at 165°E (Fig. 2). The overall mean picture along the equator is very similar to a climatology from TAO moorings (Yu & McPhaden, 1999). The thermocline also sharpens to the east as it shoals, especially off the equator (Fig. 3).

The salinity field (Fig. 4) shows the influence of heavy rain under the intertropical convergence zone (ITCZ) in the east and the warm pool in the west. Fresh surface values are found in these regions. In addition, equatorward advection of water subducted in the subtropics is evident as tongues of high salinity southern water and low salinity northern water. The tongues extend toward the equator at the level of the EUC. This high-salinity tongue in the pycnocline extends northward and westward from the southeast Pacific. The tongue is associated with equatorward thermocline flow that feeds the EUC (Johnson & McPhaden, 1999), driven by the zonal pressure gradient due to the thermocline slope. The strong meridional salinity front within the thermocline on the equator reflects equatorial convergence of these salty southern and fresher northern waters, feeding the EUC. An isolated salinity maximum is found near 80-m depth just south of the equator east of 155°W. This feature is the result of eastward advection of this salty water in the EUC, surrounded by westward advection of fresher water in both branches of the SEC. Fed from the western and central Pacific, this feature is remarkably persistent while flowing east in the EUC over 5,000 km (Fig. 4). In the west, there is a chimney of salty water near the equator that appears to extend into the mixed layer. This feature is better discussed in the context of the seasonal cycle below.

3.2 The seasonal and ENSO cycles

Seasonal and ENSO cycle variations of zonal velocity, temperature, and salinity are described along the equator and at three representative longitudes: the western Pacific at 165°E, the central Pacific at 155°W, and the eastern Pacific at 110°W. At each longitude, the zonal current variations are described, and these variations are then related to the potential temperature and salinity fields. A set of eight zonal sections at the equator is shown for each of these properties (Figs. 5–7). The top six sections are bimonthly presentations of the properties, evaluated in the middle of the month noted. These sections start with mid-February in the upper left and proceed down to mid-June, then go on to mid-August in the upper right proceeding down to mid-December. The bottom two sections show the perturbations imposed on the mean during mild El Niño conditions (SOI = -1.0) and mild La Niña conditions (SOI = +1.0). A similar convention is followed for meridional sections at the western, central, and eastern Pacific longitudes (e.g., Figs. 8–10).

There were not sufficient degrees of freedom to include semiannual harmonics with any confidence in this analysis. TAO mooring data do suggest that near-surface velocities in the western Pacific have a significant semiannual signal (Yu & McPhaden, 1999), which is missed here. Fortunately, these data also suggest that the semiannual signal on the equator is

small at depth in the west and throughout the water column in the east. A surface drifter velocity climatology is in agreement with the TAO mooring data on the importance of the semiannual harmonic on the equator in the western Pacific (Reverdin et al., 1994). In addition, this climatology suggests significant semiannual energy in both branches of the SEC in the central Pacific. The lack of a semiannual harmonic in the present work should be borne in mind, especially in these regions.

The isopycnal averaging framework allows more structure than one might expect (below the mixed layer) given the annual harmonics and the linear regression against the SOI. Since fits are made for both the potential isopycnal depths and for the properties (zonal velocity, potential temperature, and salinity) on isopycnals, there are twice as many degrees of freedom as for a similar fit on isobaths. The depth of an isopycnal and the values of properties on that isopycnal can vary in or out of phase. This potential independence in the phase and amplitude of isopycnal depth and isopycnal properties is why the data are presented using bimonthly sections, rather than by discussing the harmonic amplitudes and phases.

3.2.1 Western Pacific

At 165°E the eastward-flowing EUC peaks in June (Figs. 8 and 5), but variations in isothermal spreading about the equator associated with the seasonal cycle are not obvious (Fig. 9). Fresher surface salinities may lag the eastward surface velocities by a month (Figs. 7 and 5), perhaps a signature of eastward advection of the fresh pool from the west during this season. In contrast, the westward-flowing EIC and SEC(N) both peak in December. The eastward-flowing NECC also peaks in December, consistent with the thermocline trough between the SEC(N) and NECC being strongest during this time (Fig. 9). The SEC(S) is maximum in February–April at 165°E (Fig. 8). The current also shows a relatively weak seasonal cycle in the central Pacific (Fig. 11), and is maximum in October–December at 110°W (Fig. 14).

In February–April a chimney of salty water appears to extend upward from the subsurface salinity maximum near the equator in the western Pacific (Figs. 10 and 7). This chimney results from some combination of equatorial upwelling, westward advection of saltier water from the east (Figs. 5 and 7), seasonal changes in local precipitation, and deep mixing from strong wind events in November–March (Cronin & McPhaden, 1998).

At 165°E El Niño weakens the EUC at its core (Figs. 8 and 5), but a strong eastward surface flow develops on the equator (Cronin, McPhaden & Weisberg, 2000). The thermocline becomes shallower and relatively diffuse in the west (Figs. 6 and 9) as the warm pool is drained by eastward advection (Picaud & Delcroix, 1995). Surface salinities are fresh during El Niño as precipitation migrates east with the warm pool (Figs. 7 and 10; Delcroix & Picaud, 1998). In addition a strong NECC is present around 5°N (Fig. 8; Kessler & Taft, 1987). The EIC also appears to be stronger than normal. In contrast, La Niña conditions see a strong EUC and a strong SEC, while the NECC is pushed northward to about 7°N. In other words, during La Niña the equatorial current system is strengthened and looks more like the central Pacific than the western Pacific as the easterly trade winds migrate westward. The trades drive both the equatorial SEC (frictionally) and the EUC through the zonal pressure gradient. In addition, during La Niña there is a relatively sharp and deep thermocline as the warm pool builds in the west, in addition to salty surface conditions as the convection shifts west and advection in the SEC carries saltier central Pacific waters westward.

3.2.2 Central Pacific

At 155°W the EUC peaks in June (Figs. 11 and 5), and the contrast in the spreading of the thermocline about the equator between June and December is visible (Figs. 12 and 6). Highest EUC speeds are seen when the current is shallowest (Fig. 5), which occurs when equatorial easterly trade winds are weakest. The very strong shears above the EUC and the interaction between the eastward zonal pressure gradient and the westward surface stress indicate the complex mix of influences on the EUC (Philander & Pacanowski, 1980; McPhaden & Taft, 1988; Wacogne, 1990). At 155°W there is no surface expression of eastward equatorial flow in any season (assuming that extrapolation of the ADCP shear below 20 m to the surface adequately describes the surface velocity). Perhaps as a result, there is little change in the salinity field on the equator in the central Pacific (Figs. 13 and 7). The SEC(N) appears strongest in December, and the NECC peaks in October. This slight phase difference agrees with results from island sea level data that span the entire SEC(N) (Wyrtki, 1974a). However, this shift was not noted in other studies, which could not fully resolve the near-equatorial SEC (Kessler & Taft, 1987). The thermocline is very sharp, with a strong seasonal cycle in the strength of the trough between the SEC(N) and the NECC as these currents wax and wane. The most prominent cycle in salinity at 155°W is found in the north, under the ITCZ, with very fresh surface values in October–December.

At 155°W the ENSO cycle variation in the equatorial Pacific current system can be seen (Fig. 11) as the trades weaken during El Niño and strengthen during La Niña. The EUC and SEC are both weaker during El Niño compared to La Niña. As at 165°E, the NECC shifts southward during El Niño and northward during La Niña. Finally, the cold tongue is suppressed during El Niño and enhanced during La Niña (Figs. 12 and 6), as expected.

While the meridional shifts of the NECC and the amplitude modulation of the SEC(N) with the ENSO cycle are in accord with previous studies, the modest NECC during El Niño is not (Wyrtki, 1974b; Taft & Kessler, 1991). The sparse temporal and spatial sampling of the sections (Johnson et al., 2000) may not resolve NECC amplitude changes associated with the SOI in the central Pacific. The near-equatorial currents are strong during the boreal fall, winter and La Niña. Their strength supports the generation of TIWs in the central and eastern Pacific (Baturin & Niiler, 1997). These waves can be sufficiently vigorous that they may alias the analysis in these regions. Examination of individual sections suggests that TIWs are aliasing the currents in the central Pacific, but not so much the eastern Pacific. During the La Niña phase of the SOI, it appears that in the central Pacific TIWs are sampled preferentially in phases that reinforce the SEC(N) and NECC.

3.2.3 Eastern Pacific

At 110°W the relationships between zonal velocity, temperature, and salinity in the EUC are all evident in the seasonal cycle. The EUC peaks in strength around April, when it also surfaces (Figs. 14 and 5; Philander & Pacanowski, 1980). This far east the thermocline is extremely sharp and shallow (Fig. 15 and 6). The equatorial spreading of the thermocline associated with the EUC is noticeably stronger during April than in October, when equatorial SST is lowest and the SEC is strongest. The laterally isolated salinity maximum within the thermocline just south of the equator (Figs. 16 and 7) is strongest when the EUC velocity is a maximum, or slightly thereafter. This lagged correlation of maxima in EUC salinity and

velocity agrees with results slightly further to the east (Lukas, 1986).

In the north, the NECC is minimum in strength near 110°W (Fig. 2), with no eastward surface flow in December–February and a surface expression that peaks in August (Fig. 14). The thermocline trough between the SEC and NECC is only apparent from August to October, again concordant with the zonal velocity (Fig. 15). Interestingly, while the NECC is weak at 110°W, the NSCC and SSCC are strong. These countercurrents also display a noticeable seasonal cycle at 110°W, being stronger in the first half of the year than in the second. At 110°W surface salinities under the ITCZ are freshest in October (Fig. 16), when the ITCZ is strongest. In addition, surface salinities are fresh as far south as 7°S in December and February, advected west from fresh coastal waters by the SEC, with westward surface velocities that peak a few months earlier (Fig. 14).

As at 155°W, the current system at 110°W is spun up during La Niña, when compared to El Niño (Fig. 14). The cold tongue is much stronger during La Niña and quite weak during El Niño (Fig. 15). Surface salinities are generally fresher during El Niño than during La Niña (Fig. 16). These fresh salinities are at least partially due to local precipitation associated with eastward migration of warm sea surface temperatures and convection and part due to reduced trade winds (Ando & McPhaden, 1997).

4. Zonal current properties and their variation

The EUC, NECC, and both branches of the SEC are analyzed for each synoptic section. Quantities evaluated include zonal volume transport as well as velocity-weighted latitude, depth, potential temperature, and salinity for each current at each longitude. These quantities are estimated only where the sections have sufficient meridional and vertical coverage in currents and water properties to sample fully the current. The NECC was the least frequently sampled current by the synoptic sections, followed by the SEC(S). These quantities are then fit in the same manner as the section data discussed above.

In this analysis, the EUC is defined as all eastward flow between 2°N and 2°S (Gouriou & Toole, 1993) for potential densities of $23 < \sigma_\theta < 26.5 \text{ kg m}^{-3}$. In the west, the latitude limits help separate the EUC from the NSCC and the SSCC at depth, as well as from the surface NECC. The lighter limit helps to distinguish the EUC from transient eastward-flowing surface jets driven by local westerly wind events (Cronin, McPhaden & Weisberg, 2000), especially in the west. The denser limit attempts to distinguish the EUC from deeper eastward flows that are sometimes present below the EUC, usually separated by a velocity reversal (the EIC) or a minimum in eastward velocity.

The NECC is here defined as all eastward flow north of 2°N for $\sigma_\theta < 26.0 \text{ kg m}^{-3}$. To be used for NECC estimates, the velocity and density fields had to suggest that the northern edge of the NECC was sampled. This restriction meant that the sections usually had to reach to 8°N or beyond, which unfortunately but unavoidably creates some potential for a biased sample. The 26.0 kg m^{-3} density limit is near the base of the thermocline and helps to distinguish the NECC from the NSCC. The current separation is on the whole a bit denser than previous ones at 165°E based on the minimum in eastward velocity (Gouriou & Toole, 1993), and at 110°W based on σ_θ (Hayes, Toole & Mangum, 1983).

The SEC(N) is defined as all westward flow between the equator and the NECC, and again for $\sigma_\theta < 26.0 \text{ kg m}^{-3}$. The SEC(S) is defined as all westward flow between 8°S (because most of the sections stop at that latitude) and the equator for $\sigma_\theta < 26.0 \text{ kg m}^{-3}$. In

the far west, around 143°E, New Guinea is substituted for 8°S as the southern limit of the SEC(S). In this region, upper portions of the NGCUC are counted as part of the SEC(S). The density limit for both branches of the SEC is consistent with that for the NECC.

The synoptic analysis presents a picture different from that of the mean section analysis in at least three ways. First, in the synoptic analysis each section is reduced to a set of single parameters before fitting. Thus the fits have less structure than the mean analysis, since the mean analysis allows independent variations in the properties on isopycnals and the depth of those isopycnals. Deviations of current properties with respect to the ENSO cycle in the synoptic analysis are just linear perturbations of the mean properties regressed against the SOI and the seasonal cycle is a pure annual harmonic. Thus, only El Niño fits are shown, since La Niña fits contain no additional information. For each current and quantity the means and the variations with the ENSO cycle (shown as a strong El Niño by evaluating the fits at SOI = -1.5) are presented as functions of longitude. The seasonal cycle is shown separately.

The second difference is that the synoptic section analysis exactly follows the currents as they move horizontally and vertically, within the density and latitude limits noted above: a Lagrangian approach. However, while the mean section analysis is quasi-Lagrangian in the vertical, since it is done on isopycnals, it is closer to Eulerian in the meridional. The annual harmonics and regression against the SOI in the mean section analysis accounts for some of the currents' meridional migrations, but not all of them. That is to say, currents are not completely followed as they move north or south with various higher frequency motions such as TIWs and other disturbances.

The third difference is that the synoptic section analysis defines currents as all flow in a given direction and region as noted above. With this definition, there are never current reversals in individual sections, just absences of currents, which are fit as zero transport and omitted from the other property fits. This situation contrasts with the mean section analysis which includes velocity reversals at any given latitude and isopycnal. These last two differences combine for stronger current transports in the fits of the synoptic section analysis than in the mean section analysis.

4.1 Zonal current volume transports

Variations of the equatorial zonal currents are closely connected to seasonal and ENSO cycle changes in the equatorial easterlies. Equatorial zonal winds affect the surface currents primarily through downwind frictional forcing and setup of a zonal pressure gradient, which exerts an upwind forcing below the frictional layer. Thus, when the easterly trade winds are strong, they tend to spin up both the westward SEC at the surface and, after time, the eastward EUC beneath. By elevating the equatorial thermocline (through upwelling caused by local Ekman divergence and non-local wave adjustments), strong trades also tend to produce meridional pressure gradients that foster westward off-equatorial currents. During El Niño, or during the phase of the annual cycle with westerly anomalies, the opposite changes occur.

The mean volume transport of the EUC (Figs. 17 and 5) is larger in the central Pacific than in the west or the east. In the central Pacific the trade winds are strongest, the zonal thermocline slope and thus the zonal pressure gradient is the biggest, and so the EUC is the largest. The seasonal cycle in EUC transport is substantial at all longitudes. The phasing is such that EUC transport peaks in mid-May in the east and late June in the west, as the

relaxed trade winds during this time allow increased eastward flow in the upper half of the EUC (Philander, Hurlin & Seigel, 1987). This westward phase propagation in the EUC agrees with model results (Blanke & Raynaud, 1997) and empirical analyses (Yu & McPhaden, 1999). The weakening or disappearance of the EUC during the height of El Niño has been observed during the events of 1982–83 (Firing, Lukas, Sadler & Wyrski, 1983), 1986–87 (McPhaden, Hayes, Mangum & Toole, 1990), 1991–92 (Kessler & McPhaden, 1995) and 1997–98 (Johnson et al., 2000).

The mean transport of the NECC is fairly constant over the western and central Pacific, but decreases in the east, becoming smallest around 110°W (Fig. 17). This minimum at 110°W is as expected from the Sverdrup relation (Kessler, 2001). The sampling in the far west is sparse and the transport uncertainties are correspondingly large. The seasonal cycle is a large fraction of the mean transport of the NECC. The NECC has its largest transport in August at 95°W, but at and west of 125°W the maximum in transport is in October–December, except near 143°E, which probably sees the influence of the western boundary. This shift with longitude is again a signature of westward phase propagation. Around February the NECC is very weak east of 125°W. During El Niño events, the NECC is important for export of water eastward from the warm pool, and its transport increases about 25% (Picaut, Ioualalen, Menkes, Delcroix & McPhaden, 1996). Central Pacific transport NECC variations with the SOI are aliased by TIWs as discussed in Section 3.2.

Transport estimates for the westward-flowing SEC(N) are difficult and rarely direct (Wyrski, 1974a; Wyrski & Kilonsky, 1984; Picaut & Tournier, 1991). The mean volume transport of this current peaks in amplitude in the central Pacific (Fig. 17). Throughout the basin, but especially in the western Pacific where the NECC is closest to the equator, the SEC(N) is sometimes absent. The current transport estimated through the synoptic analysis in the west is clearly large compared with the mean fields estimated on isopycnals (Fig. 8). This example best highlights this difference between the synoptic current transport analysis and the mean fit fields as discussed in Section 4.

Much like the NECC, the seasonal cycle of the SEC(N) volume transport is such that the current is weakest in February–March in the east, but this lull transitions to around July in the west (Fig. 17; Wyrski, 1974a). Depth fluctuations of the thermocline trough near 4°N–5°N affect both the SEC(N) to the south and the NECC to the north, by modulating the pressure gradients across both currents simultaneously. As a result, their transport variations tend to be approximately in phase (Kessler & Taft, 1987). The local manifestation of an annual equatorial Rossby wave at 5°N (Yu & McPhaden, 1999) accounts for most of the annual variability of the depth of the trough (Kessler, 1990). This wave is forced by the wind stress curl due to the annual north-south migration of the ITCZ. The amplitude of the seasonal cycle is large throughout the basin. Unfortunately, the SEC(N) and NECC transport estimates around 140°W are aliased by energetic TIWs sometimes present in the central Pacific as discussed in Section 3.2.2. The TIW signal is reflected by the relatively wide distribution of transport estimates for these currents in that region (Fig. 17).

West of 110°W, the SEC(N) is greatly reduced during El Niño, at least partly due to the reduced trades. Equatorial thermocline deepening reduces the meridional pressure gradient and results in anomalously eastward surface geostrophic velocities during El Niño, with a reduced SEC and an increased NECC. Momentum advection driven by cross-equatorial southerly winds may also be important in the SEC(N) dynamics in the central to eastern Pacific (Philander et al., 1987).

The SEC(S) mean volume transports (Fig. 17) build from fairly small values at 95°W to nearly constant values west of 140°W, before diminishing again west of 165°E. As mentioned before, at 143°E the upper part of the NGCUC is folded into these SEC(S) transport estimates. The amplitude of the seasonal cycle is large only from 165°E to 155°W, with the current being strongest in February–March, roughly in opposite phase with the SEC(N). The volume transport decreases significantly only in the west during El Niño (except at 143°E where the NGCUC is strong during that phase of ENSO). This change is a different, and much less dramatic, response to reduced trade wind forcing than that seen in the SEC(N). The zonal asymmetry may be due to an enhancement of the South Pacific Convergence Zone (SPCZ) during El Niño, which increases the SECC and reduces the SEC(S) in the western Pacific (Kessler & Taft, 1987). It is important to remember that there may be SEC(S) fluctuations beyond 8°S that are missed by this data set.

4.2 Zonal current latitudes and depths

The mean latitude of the EUC (Figs. 18 and 2) is near the equator except at 143°E where the NGCUC is strong. The EUC core shifts slightly south of the equator in the east, owing to the meridional circulation induced by predominantly southerly winds in that region (Philander & Delecluse, 1983; Kessler, Rothstein & Chen, 1998). Eastward shoaling of the EUC is apparent in the mean from 143°E to 125°W, but the velocity-weighted EUC is relatively constant in depth east of that longitude (Fig. 19) while the peak velocity continues to shoal slightly (Fig. 3).

The seasonal cycle of EUC depth is very smooth and well defined. The current shoals in March at 95°W, and this shoaling generally lags to the west (except closest to the western boundary), with maximum shoaling in August by 165°E. This westward propagation is a signature of an annual Rossby wave (Lukas & Firing, 1985; Kessler & McCreary, 1993). Shallower depths are generally associated with large transports in the seasonal cycle, although there are some phase differences between seasonal EUC transport and depth. This correlation arises as the EUC picks up eastward transport in the shallower layers with relaxed trade winds. The seasonal cycle of EUC latitude is very small except in the far west. During El Niño the EUC shifts northward toward the equator in the central Pacific. During this phase of ENSO the EUC deepens considerably in the east, and shoals in the west, consistent with the reduced zonal slope of the equatorial thermocline.

The mean latitude of the NECC moves gradually northward as the current progresses from west to east, with an interruption of this tendency at 110°W (Figs. 18 and 2), where the mean transport is weakest (Fig. 17). At this longitude the NECC and NSCC are difficult to distinguish because the NECC is very weak, so there is little eastward velocity above the thermocline. The NECC also shoals from west to east (Fig. 19) with the shoaling thermocline. The seasonal cycle of latitude is such that the NECC is generally found furthest south when its volume transport is at a minimum. The seasonal cycle of depth is notable only west of 125°W, with the current being slightly deeper in February–April. During El Niño the NECC is found south of its usual latitude in the western and central Pacific, and it shoals in the western Pacific with a hint of deepening in the east, as expected from the migration of the warm pool to the east during this phase of ENSO.

The mean latitude of the SEC(N) starts near 2°N in the east, approaches 3°N in the central Pacific (Figs. 18 and 2), where the current is strongest, and then tends southward to

1°N in the west where the current weakens. The SEC(N) also deepens to the west (Fig. 19), again with the westward deepening of the thermocline until it reaches the warm pool, where the depth remains constant. The seasonal cycle of latitude is such that the SEC(N) is generally furthest north when its volume transport is at a minimum, in contrast with the seasonal cycle of the NECC. The current is shallowest in January–February in the east, with a westward lag toward shallowest values in May–June in the west. Deeper values are correlated with larger transports. During El Niño the current moves southward as it weakens in transport, again consistent with eastward migration of the warm pool. Interestingly, during El Niño it also deepens in the west as its transport decreases, because surface flow tends to be eastward during this time and the SEC(N) is sometimes limited to a subsurface expression.

The SEC(S) is located from 4°S to 5°S in the mean (Fig. 18), except near the western boundary where it is forced northward by New Guinea and joins the NGCUC. Of course, this latitude is somewhat influenced by the southern limit of 8°S in this analysis. Like the rest of the currents, the SEC(S) deepens to the west (Fig. 19) with the thermocline. In the seasonal cycle, the SEC(S) also generally shifts south when transports are weakest. The seasonal cycle of the SEC(S) depth is such that it is shallowest in May–August, roughly in phase with the SEC(N). The current shifts southward in the west and weakens under El Niño conditions. During El Niño, like the SEC(N), the current deepens (except in the far west where the NGCUC influences the analysis) for the same reason; a tendency toward increased eastward surface flows.

4.3 Zonal current temperatures and salinities

In the mean the EUC is warmest (Fig. 20) and saltiest (Fig. 21) near the dateline. These changes occur because the current adds warm and salty water from the southern hemisphere (Johnson & McPhaden, 1999) as it moves eastward, but then as it surfaces in the east its warmer and saltier waters upwell into the SEC. The seasonal cycle is such that the EUC is warmer and saltier when the transport is largest, because the upper layers of the EUC, which are warmer and saltier, make up most of the seasonal variability. During El Niño there is some warming of the EUC in the eastern Pacific, owing to more near-surface eastward flow under the relaxed trades. During El Niño there is also some freshening of the EUC in the western Pacific, perhaps associated with eastward migration of the fresh pool in the upper portions of the EUC.

The NECC temperature is relatively warm (Fig. 20) and fresh (Fig. 21), but it cools a little and freshens a lot in the mean as it flows eastward under the high precipitation of the ITCZ. The seasonal cycle is such that the NECC is warmest and freshest when the transports are largest, because near-surface intensification accounts for much of the seasonal cycle. The NECC tends to be warmer in the east during El Niño, and fresher in the central Pacific during this time. The latter change is probably due to large-scale precipitation changes and eastward advection of the fresh pool.

The SEC(N) is cool (Fig. 20) and fresh (Fig. 21) in the east where it sits adjacent to the ITCZ and fresh coastal surface waters. It warms and becomes increasingly salty to the west. The seasonal cycle of temperature is such that larger transports are generally associated with cooler temperatures. The seasonal cycle of salinity is really only large in the east, where the current is freshest in January, a time when its transport is low and the ITCZ has moved south over the current. As might be expected, the SEC(N) is slightly warmer in the east

during El Niño, when the cold equatorial upwelling that feeds it is suppressed. The salinity shows no change with variations of the ENSO cycle.

Like the SEC(N), the SEC(S) warms (Fig. 20) and gets saltier (Fig. 21) as it transits from east to west, except that it cools slightly and freshens in the far west, due to the presence of the SPCZ. The exception is the western boundary where the cold, relatively fresh influence of the NGCUC is seen. The current is generally warmest around April throughout the basin. However, it is saltiest in the eastern Pacific around July when the ITCZ is far to the north, and freshest in the western Pacific around the same time. During El Niño the current warms slightly in the east, again not surprising since it is fed at least in part from equatorial and coastal upwelling, both of which are much weaker and warmer during El Niño. The SEC(S) also gets a bit saltier in the central Pacific during El Niño, mostly because the current deepens. In addition, it is found only well south of the equator then. With these changes the current carries a lower fraction of fresher surface equatorial water.

5. Conclusion

Meridional sections constructed from contemporaneous CTD and ADCP data taken across the Pacific, primarily during the 1990's, have been used to describe the mean zonal evolution of upper-ocean tropical zonal velocity, temperature, and salinity, as well as the seasonal cycle and the ENSO cycle. The data are unusual in that they allow direct estimates of properties of the near-equatorial currents, including the SEC(N), EUC, and EIC. The large number of sections taken, and the quality of the zonal velocity data, enable a four-dimensional exploration of the upper ocean zonal velocity field. The analysis should be useful for model comparisons. In addition it comprises a consistent climatology of simultaneously sampled zonal velocity, temperature, and salinity for the decade, to compare with past and future decades.

Some of the more novel results of this analysis involve the near-equatorial and subthermocline currents. For instance, the westward intensification of the EIC stands out in the mean velocity sections. A seasonal cycle of the EIC may also be seen in the west. Another intriguing result in the eastern Pacific is a hint of a seasonal cycle of the SCCs at 110°W. Basin-wide estimates of the SEC(N) and its properties are unusual. The SEC(N) has a central Pacific transport maximum, a seasonal cycle nearly in phase with the NECC, and the suggestion of a large reduction during El Niño. The inclusion of so many realizations of the NGCUC in the analysis is also rare. The use of direct velocity data also allows inclusion of ageostrophic effects both around the equator (Joyce et al., 1988) and away from it. For instance, the subsurface velocity maximum in the NECC is some combination of the wind-driven Ekman layer and geostrophic shear, a feature that geostrophic calculations alone would not resolve.

These data also are the backbone for an inverse model of the tropical Pacific circulation. They are being combined with meridional velocities estimated through geostrophy and Ekman dynamics, and the entire current system is adjusted to conserve mass, heat, and freshwater, including the contributions of surface fluxes. The model is initially being run using the mean fields, but will soon include a seasonal cycle. The results are allowing diagnosis of the effects of diapycnal mixing processes on maintenance of the cold tongue. In addition, the role of the subtropical cell in cycling water from the South Pacific to the North Pacific to feed the Indonesian throughflow is being explored.

Acknowledgments. This work was partially funded by the NOAA Office of Oceanic and Atmospheric Research, the NOAA Office of Global Programs, and the NASA Physical Oceanography Program. This work was performed while BMS held a National Research Council Research Associateship Award at NOAA's Pacific Marine Environmental Laboratory (PMEL). The analysis would not have been possible without the careful and sustained work of the TAO project, especially the officers, crew, and scientific parties of the NOAA Ships *Discoverer*, *Ka'imimoana* and *Ronald H. Brown*, especially Dennis Sweeny. Eric Johnson and Patricia Plimpton processed the earlier NOAA ADCP data. June Firing and Jules Hummon processed the later NOAA ADCP data as well as much of the ADCP data from other sources. Data from R/V *Kaiyo* were also essential, with contributions from the officers, crew, and all TOCS participants both at sea and ashore. Discussions with Mike McPhaden were useful. PMEL Contribution Number 2337.

REFERENCES

- Akima, H. (1970). A new method of interpolation and smooth curve fitting based on local procedures. *Journal of the Association for Computing Machinery*, 17, 589–602.
- Ando, K., & McPhaden, M.J. (1997). Variability of surface layer hydrography in the tropical Pacific Ocean. *Journal of Geophysical Research*, 102, 23,063–23,078.
- Baturin, N.G., & Niiler, P.P. (1997). Effects of instability waves in the mixed layer of the equatorial Pacific. *Journal of Geophysical Research*, 102, 27,771–27,793.
- Blanke, B., & Raynaud, S. (1997). Kinematics of the Equatorial Undercurrent: An Eulerian and Lagrangian approach from GCM results. *Journal of Physical Oceanography*, 27, 1038–1053.
- Bryden, H.L., & Brady, E.C. (1985). Diagnostic model of the three-dimensional circulation in the upper equatorial Pacific Ocean. *Journal of Physical Oceanography*, 6, 33–37.
- Butt, J., & Lindstrom, E., (1994). Currents off the east coast of New Ireland, Papua New Guinea, and their relevance to regional undercurrents in the Western Equatorial Pacific Ocean. *Journal of Geophysical Research*, 99, 12,503–12,514.
- Cornuelle, B.D., Morris, M.Y., & Roemmich, D.H. (1993). An objective mapping method for estimating geostrophic velocity from hydrographic sections including the equator. *Journal of Geophysical Research*, 98, 18,109–18,118.
- Cronin, M.F., & McPhaden, M.J. (1998). Upper ocean salinity balance in the western equatorial Pacific. *Journal of Geophysical Research*, 103, 27,567–27,587.
- Cronin, M.F., McPhaden, M.J., & Weisberg, R.H. (2000). Wind-forced reversing jets in the western equatorial Pacific. *Journal of Physical Oceanography*, 30, 657–676.
- Delcroix, T., Eldin, G., & Henin, C. (1987). Upper ocean water masses and transports in the western tropical Pacific (165°E). *Journal of Physical Oceanography*, 17, 2248–2262.
- Delcroix, T., Eldin, G., Radenac, M.-H., Toole, J., & Firing, E., (1992). Variations of the western equatorial Pacific Ocean, 1986–1988. *Journal of Geophysical Research*, 97, 5423–5445.
- Delcroix, T., & Henin, C., (1988). Observations of the equatorial intermediate current in the western Pacific Ocean (165°E). *Journal of Physical Oceanography*, 18, 363–366.
- Delcroix, T., & Picaut, J. (1998). Zonal displacement of the western equatorial Pacific "fresh pool." *Journal of Geophysical Research*, 103, 1087–1098.

- Donguy, J.-R., & Meyers, G. (1996). Mean annual variation of transport of major currents in the tropical Pacific Ocean. *Deep-Sea Research I*, 43, 1105–1122.
- Eldin, G. (1983). Eastward flows of the south equatorial central Pacific. *Journal of Physical Oceanography*, 13, 1461–1467.
- Eldin, G., Delcroix, T., Henin, C., Richards, K., du Penhoat, Y., Picaut, J., & Rual, P. (1994). The large-scale structure of currents and hydrology along 156°E during the COARE Intensive Observation Period. *Geophysical Research Letters*, 21, 2681–2684.
- Firing, E., Lukas, R., Sadler, J., & Wyrtki, K. (1983). Equatorial undercurrent disappears during the 1982–83 El Niño. *Science*, 222, 1121–1123.
- Firing, E., Wijffels, S.E., & Hacker, P. (1998). Equatorial subthermocline currents across the Pacific. *Journal of Geophysical Research*, 103, 21,413–21,423.
- Gouriou, Y., & Toole, J. (1993). Mean circulation of the upper layers of the western equatorial Pacific Ocean. *Journal of Geophysical Research*, 98, 22,495–22,520.
- Hayes, S.P. (1982). A comparison of geostrophic and measured velocities in the Equatorial Undercurrent. *Journal of Marine Research*, 40, Suppl., 219–229.
- Hayes, S.P., Mangum, L.J., Picaut, J., Sumi, A., & Takeuchi, K. (1991). TOGA-TAO: A moored array for real-time measurements in the tropical Pacific Ocean. *Bulletin of the American Meteorological Society*, 72, 339–347.
- Hayes, S.P., Toole, J.M. & Mangum, L.J. (1983). Water-mass and transport variability at 110°W in the equatorial Pacific. *Journal of Physical Oceanography*, 13, 153–168.
- Johnson, E.S., & Luther, D.S. (1994). Mean zonal momentum balance in the upper and central equatorial Pacific Ocean. *Journal of Geophysical Research*, 99, 7689–7705.
- Johnson, E.S., & Plimpton, P.E. (1999). *TOGA/TAO shipboard ADCP data report, 1991–1995*. NOAA Data Rep., ERL PMEL-67, 23 pp.
- Johnson, G.C., (2001). The Pacific Ocean subtropical cell surface limb. *Geophysical Research Letters*, 28, 1771–1774.
- Johnson, G.C., McPhaden, M.J., & Firing, E. (2001). Equatorial Pacific Ocean horizontal velocity, divergence, and upwelling. *Journal of Physical Oceanography*, 31, 839–849.
- Johnson, G.C., & McPhaden, M.J. (1999). Interior pycnocline flow from the subtropical to the equatorial Pacific Ocean. *Journal of Physical Oceanography*, 29, 3073–3098.
- Johnson, G.C., McPhaden, M.J., Rowe, G. D., & McTaggart, K.E. (2000). Upper equatorial Pacific Ocean current and salinity variability during the 1996–1998 El Niño–La Niña cycle. *Journal of Geophysical Research*, 105, 1037–1053.
- Johnson, G.C., & Moore, D.W. (1997). The Pacific Subsurface Countercurrents and an inertial model. *Journal of Physical Oceanography*, 27, 2448–2459.
- Joyce, T.M., Lukas, R., & Firing, E. (1988). On the hydrostatic balance and equatorial geostrophy. *Deep-Sea Research*, 35, 1255–1257.
- Kashino, Y., Hase, H., Ando, K., Yoneyama, K., Takatsuki, Y., Kuroda, Y., & Mizuno, K. (2001) *TOCS Data Report 2: 1995–2000*. Ocean Observations and Research Department, Japan Marine Science and Technology Center, 2-15 Natsushima Yokosuka, 237-0061, Japan, TOCS No. 4, 327 pp.
- Kessler, W.S. (1990). Observations of long Rossby waves in the northern tropical Pacific. *Journal of Geophysical Research*, 95, 5183–5217.
- Kessler, W.S. (1999). Interannual variability in the subsurface high-salinity tongue south of the equator at 165°E. *Journal of Physical Oceanography*, 29, 2038–2049.
- Kessler, W.S. (2001). Mean three-dimensional circulation in the northeast tropical Pacific.

- Journal of Physical Oceanography*, submitted.
- Kessler, W.S., & McCreary, J.P. (1993). The annual wind-driven Rossby wave in the subthermocline equatorial Pacific. *Journal of Physical Oceanography*, 23, 1192–1207.
- Kessler, W.S., & McPhaden, M.J. (1995). The 1991–93 El Niño in the central Pacific. *Deep-Sea Research II*, 42, 295–333.
- Kessler, W.S., Rothstein, L.M., & Chen, D. (1998). The annual cycle of SST in the eastern tropical Pacific, as diagnosed in an ocean GCM. *Journal of Climate*, 11, 777–799.
- Kessler, W.S., & Taft, B.A. (1987). Dynamic heights and zonal geostrophic transports in the central tropical Pacific during 1979–84. *Journal of Physical Oceanography*, 17, 97–122.
- Lagerloef, G.S.E., Mitchum, G.T., Lukas, R.B., & Niiler, P.P. (1999) Tropical Pacific near-surface currents estimated from altimeter, wind, and drifter data. *Journal of Geophysical Research*, 104, 23,313–23,326.
- Lozier, M.S., McCartney, M.S., & Owens, W.B. (1994). Anomalous anomalies in averaged hydrographic data. *Journal of Physical Oceanography*, 24, 2624–2638.
- Lukas, R. (1986). The termination of the Equatorial Undercurrent in the Eastern Pacific. *Progress in Oceanography*, 16, 63–90.
- Lukas, R., & Firing, E. (1984). The geostrophic balance of the Pacific Equatorial Undercurrent, *Deep-Sea Research*, 31, 61–66.
- Lukas, R., & Firing, E. (1985). The annual Rossby wave in the central equatorial Pacific Ocean. *Journal of Physical Oceanography*, 15, 55–67.
- McPhaden, M.J., Busalacchi, A.J., Cheney, R., Donguy, J.-R., Gage, K.S., Halpern, D., Ji, M., Julian, P., Meyers, G., Mitchum, G.T., Niiler, P.P., Picaut, J., Reynolds, R.W., Smith, N., & Takeuchi, K., (1998). The Tropical Ocean-Global Atmosphere (TOGA) observing system: A decade of progress. *Journal of Geophysical Research*, 103, 14,169–14,240.
- McPhaden, M.J., Hayes, S.P., Mangum, L.J., & Toole, J.M., (1990). Variability in the western equatorial Pacific during the 1986-87 El Niño/Southern Oscillation event. *Journal of Physical Oceanography*, 20, 190-208.
- McPhaden, M.J., & Taft, B.A. (1988). Dynamics of seasonal and interannual variability in the eastern equatorial Pacific. *Journal of Physical Oceanography*, 18, 1713–1732.
- McTaggart, K.E., & Johnson, G.C. (1999). *CTD measurements during 1997 and 1998 as part of the Global Ocean-Atmosphere-Land System (GOALS)/Pan American Climate Studies (PACS)*. NOAA Data Report ERL PMEL-66, 770 pp.
- Merle, J., Rotschi, H., & Voituriez, B. (1969). Zonal circulation in the tropical western South Pacific at 170°E. *Bulletin of the Japanese Society of Scientific Fisheries, Special Number (Professor Uda's commemorative papers)*, 91-98.
- Moum, J.N., Chereskin, T.K., Park, M.M., & Regier, L.A., (1987) Monitoring geostrophic currents at the equator, *Deep-Sea Research*, 34, 1149–1161.
- Murray, J.W., Johnson, E., & Garside, C. (1995). A U.S. JGOFS Process Study in the equatorial Pacific (EqPac). Introduction. *Deep-Sea Research II*, 42, 275–293.
- Philander, S.G.H., & Delecluse, P. (1983). Coastal currents in low latitudes (with application to the Somali and El Niño currents). *Deep-Sea Research*, 30, 887–902.
- Philander, S.G.H., Hurlin, W.J., & Seigel, A.D. (1987). Simulation of the seasonal cycle of the tropical Pacific Ocean. *Journal of Physical Oceanography*, 17, 1986–2002.
- Philander, S.G.H., & Pacanowski, R.C. (1980). The generation of equatorial currents. *Journal*

- of *Geophysical Research*, 91, 14,207–14,211.
- Picaut, J., & Delcroix, T. (1995). Equatorial wave sequence associated with warm pool displacements during the 1986–1989 El Niño–La Niña. *Journal of Geophysical Research*, 100, 18,393–18,408.
- Picaut, J., Hayes, S.P., & McPhaden, M.J., (1989). Use of the geostrophic approximation to estimate time-varying zonal currents at the equator. *Journal of Geophysical Research*, 94, 3228–3236.
- Picaut, J., Ioualalen, M., Menkes, C., Delcroix, T., & McPhaden, M.J., (1996). Mechanism of the zonal displacements of the Pacific warm pool: implications for ENSO. *Science*, 274, 1486–1489.
- Picaut, J., & Tournier, R. (1991). Monitoring the 1979–1985 Equatorial Pacific current transports with expendable bathythermograph data. *Journal of Geophysical Research*, 96, 3263–3277.
- Reid, J.L. (1959). Evidence of a South Equatorial Countercurrent in the Pacific. *Nature*, 184, 209–211.
- Reid, J.L. (1961). On the geostrophic flow at the surface of the Pacific Ocean with respect to the 1000-db surface. *Tellus*, 13, 489–502.
- Reverdin, G., Frankignoul, C., Kestenare, E., & McPhaden, M.J. (1994). Seasonal variability in the surface currents of the equatorial Pacific. *Journal of Geophysical Research*, 99, 20,323–20,344.
- Rowe, G.D., Firing, E., & Johnson, G.C. (2000). Pacific Equatorial Subsurface Countercurrent velocity, transport, and potential vorticity. *Journal of Physical Oceanography*, 30, 1172–1187.
- Taft, B.A., & Kessler, W.S. (1991). Variations of zonal currents in the central tropical Pacific during 1970 to 1987). Sea level and dynamic height measurements. *Journal of Geophysical Research*, 96, 12,599–12,618.
- Tsuchiya, M. (1975). Subsurface countercurrents in the eastern equatorial Pacific Ocean. *Journal of Marine Research*, 33, Suppl., 145–175.
- Tsuchiya, M., Lukas, R., Fine, R.A., Firing, E., & Lindstrom, E. (1989). Source waters of the Pacific Equatorial Undercurrent. *Progress in Oceanography*, 23, 101–147.
- Vintzileos, A., Delecluse, P., & Sadourny, R. (1999). On the mechanisms in a tropical ocean–global atmosphere coupled general circulation model. Part I: mean state and the seasonal cycle. *Climate Dynamics*, 15, 43–62.
- Wacogne, S. (1990). On the difference in strength between the Atlantic and Pacific undercurrents. *Journal of Physical Oceanography*, 20, 792–799.
- Webster, P. J., & Lukas, R. (1992). TOGA-COARE: The coupled ocean-atmosphere response experiment. *Bulletin of the American Meteorological Society*, 73, 1377–1416.
- Wyrtki, K. (1974a). Sea level and the seasonal fluctuations of the equatorial currents in the western Pacific Ocean. *Journal of Physical Oceanography*, 4, 91–103.
- Wyrtki, K. (1974b). Equatorial currents in the Pacific 1950 to 1970 and their relation to the trade winds. *Journal of Physical Oceanography*, 4, 372–380.
- Wyrtki, K., & Kilonsky, B. (1984). Mean water and current structure during the Hawaii-to-Tahiti shuttle experiment. *Journal of Physical Oceanography*, 14, 242–254.
- Yu, X., & McPhaden, M.J., (1999). Seasonal variability in the equatorial Pacific. *Journal of Physical Oceanography*, 29, 925–947.

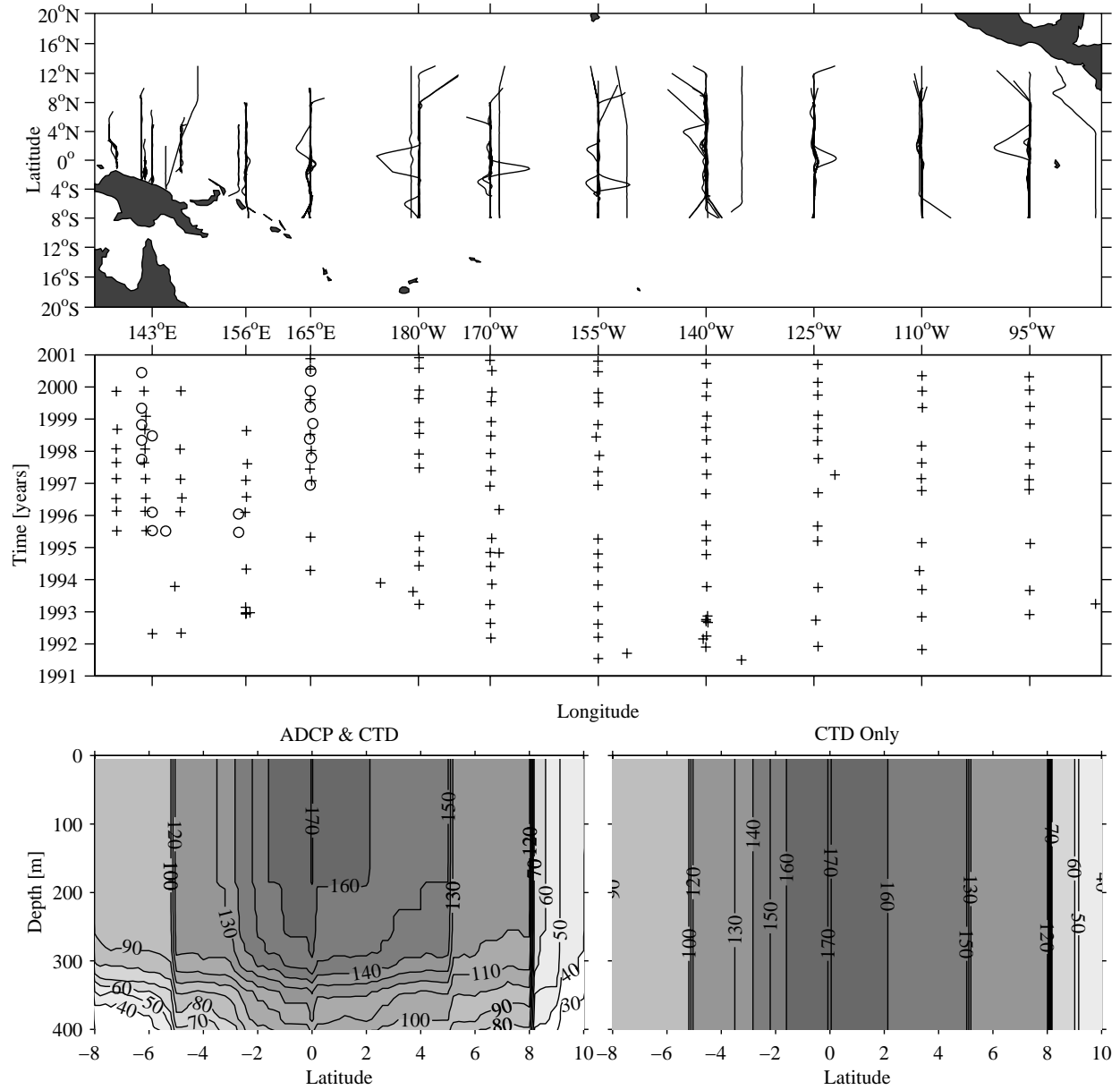


Fig. 1. CTD/ADCP section data distribution. Top panel shows latitudes and longitudes of the 172 meridional sections used in this study. Middle panel shows times when these sections crossed the equator. Sections occupied between 1991 and 2001 are shown by (+'s). Sections occupied between 1985 and 1991 are shown by (o's), with 10 years added for compactness. Bottom left panel shows (contoured at intervals of 10 with increasingly dark contours indicating more data) number of sections where ADCP and CTD data are available in the meridional-vertical plane. Bottom right panel follows bottom left but for number of sections with CTD data alone.

This page is left intentionally blank for better viewing of Figs. 2-4 in double-sided copies.

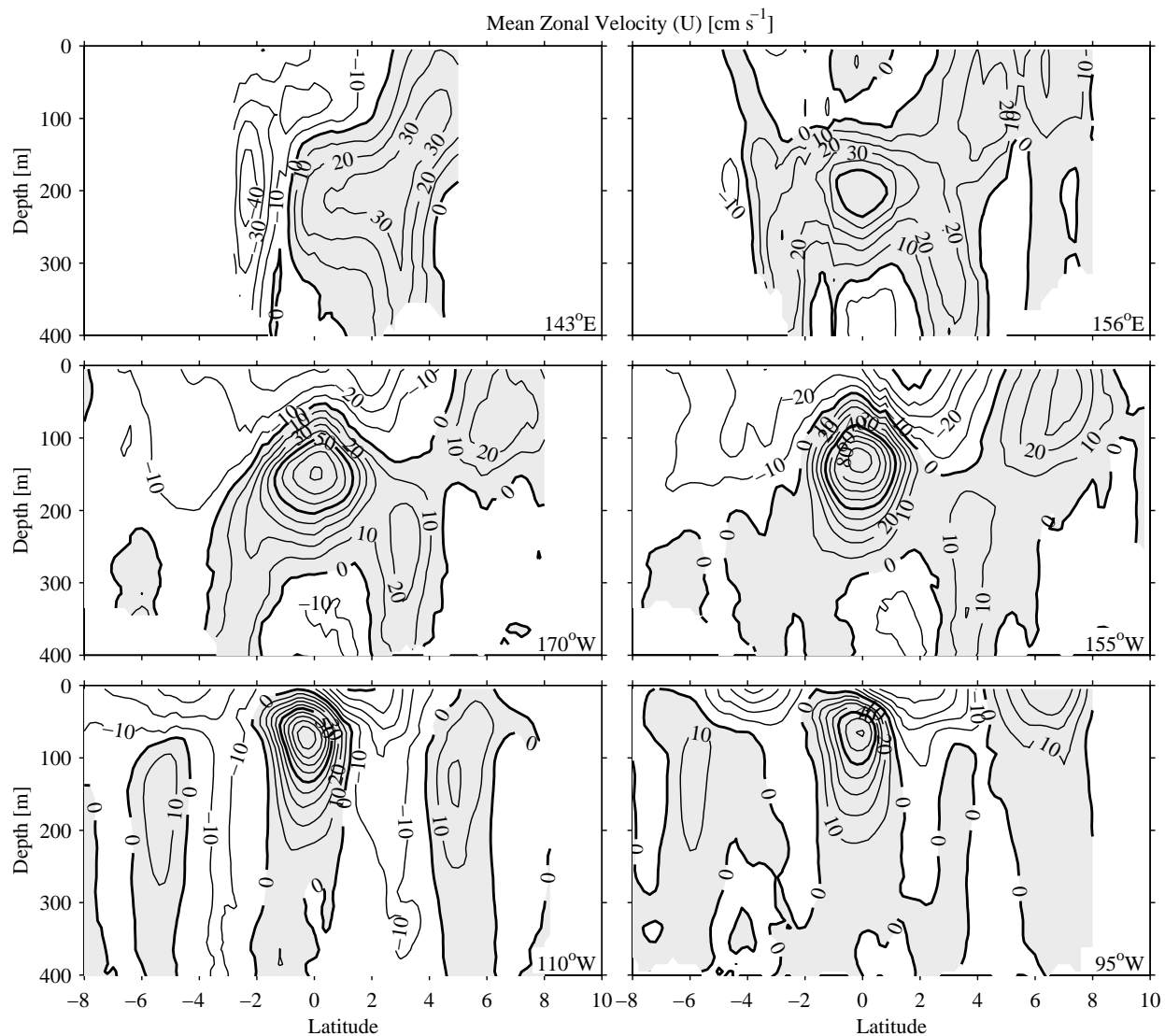


Fig. 2 (left). Sections of mean zonal velocity (u) estimated at 10 nominal longitudes and along the equator. Locations marked in the bottom right corner of each section. Contour interval is 10 cm s^{-1} , with heavy contours at 50 cm s^{-1} intervals. Eastward velocities are shaded.

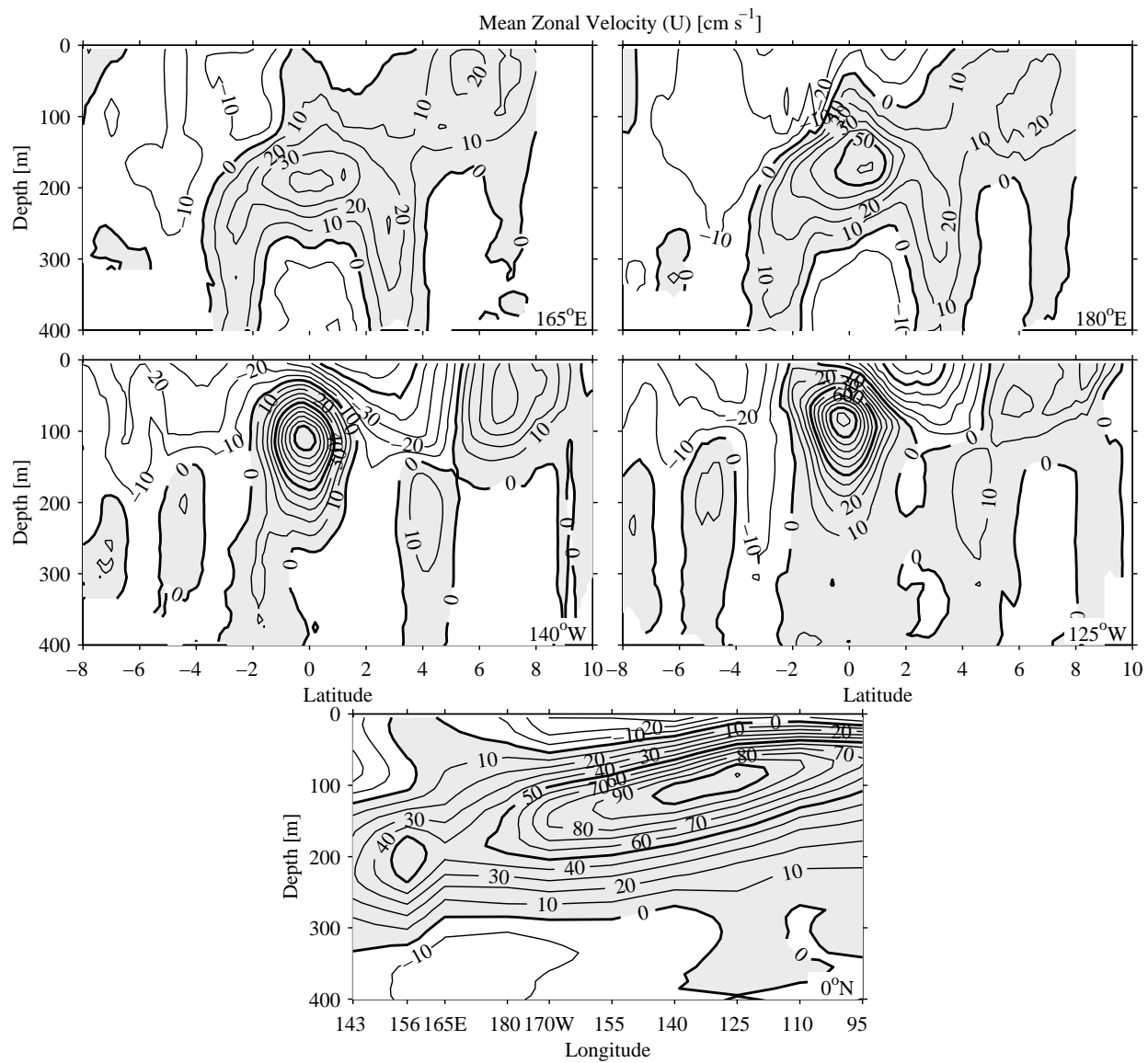


Fig. 2 (right).

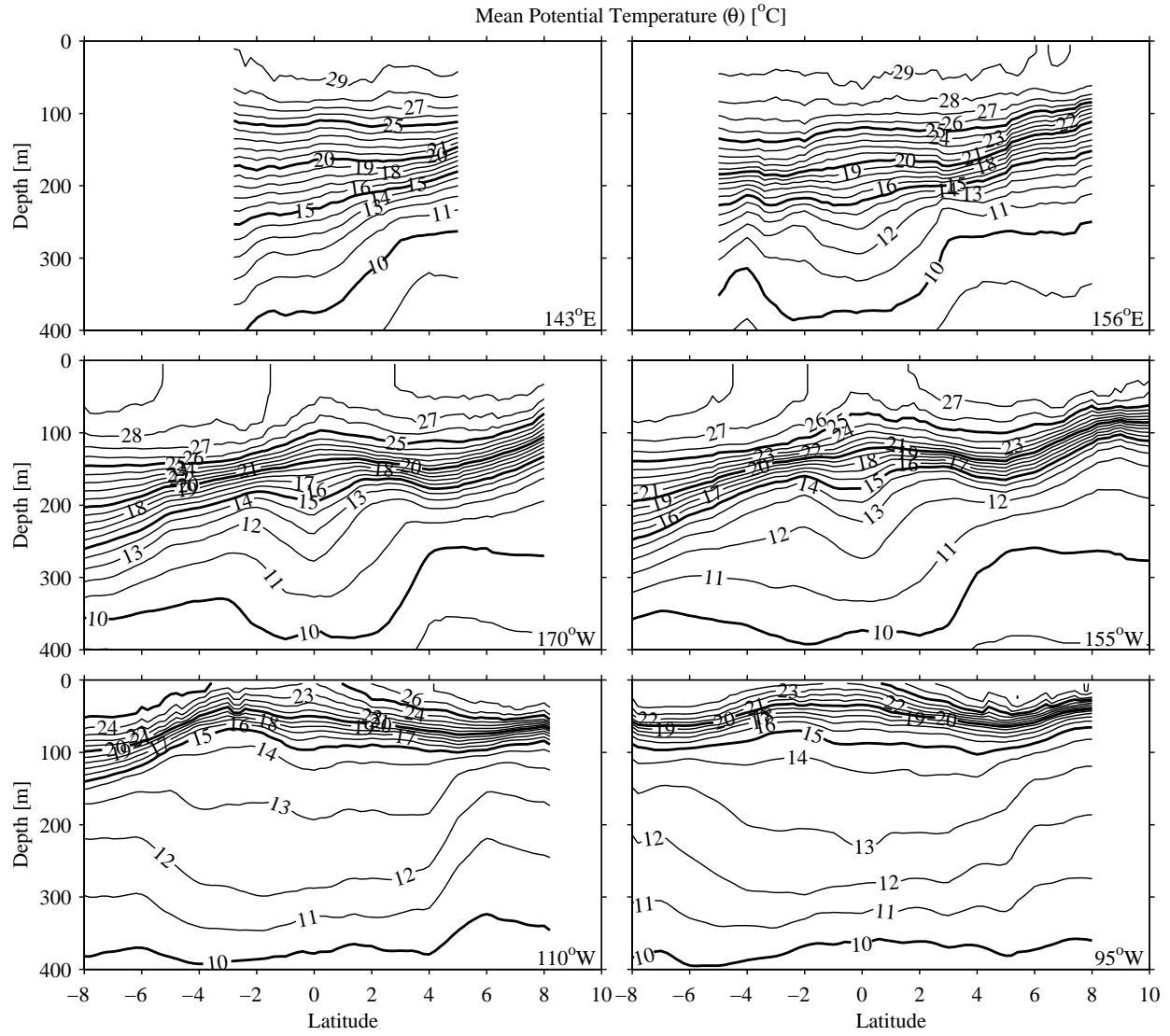


Fig. 3 (left). Sections of mean potential temperature (θ) estimated at 10 nominal longitudes and along the equator, following Fig. 2. Contour interval is 1°C , with heavy contours at 5°C .

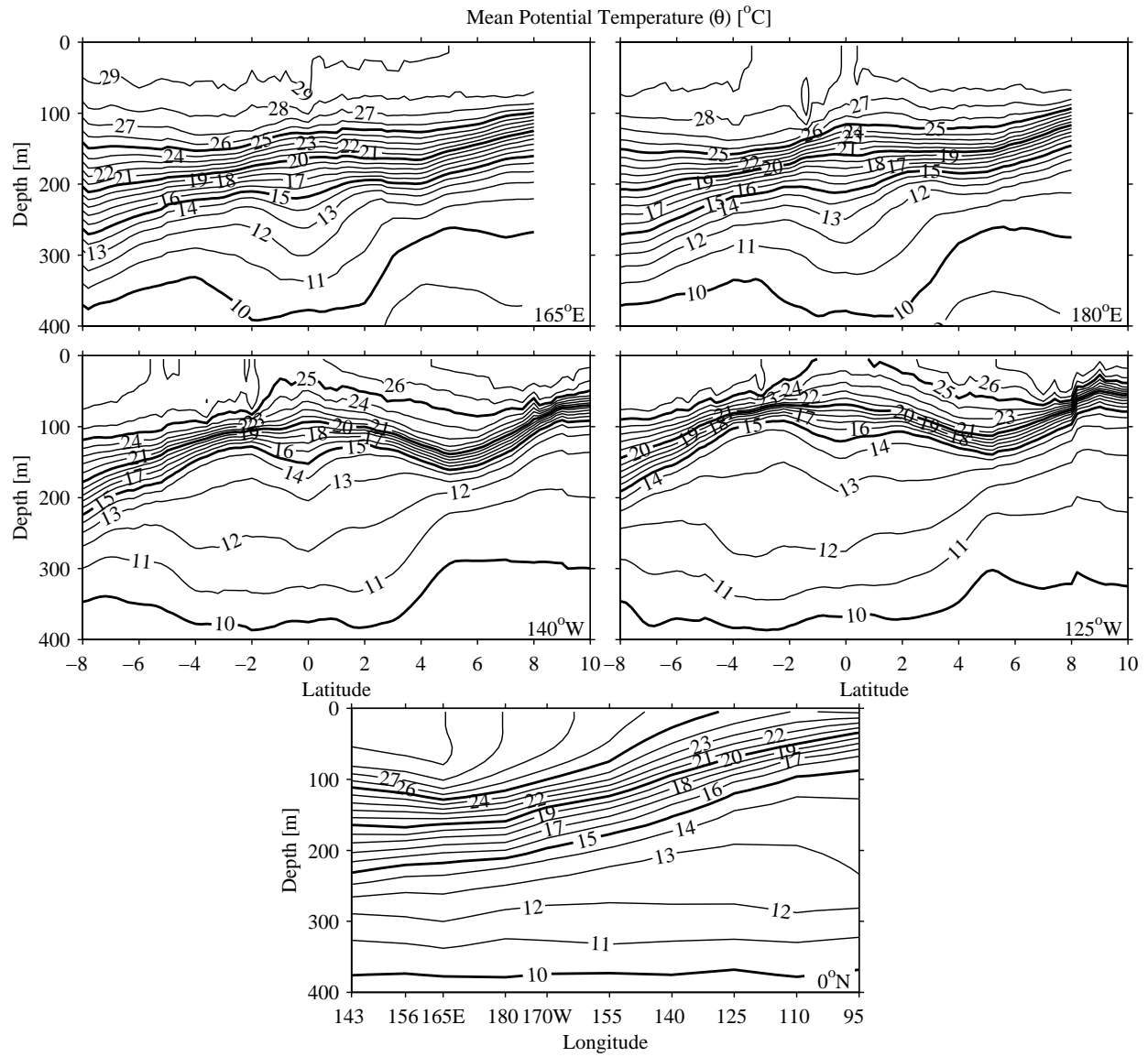


Fig. 3 (right).

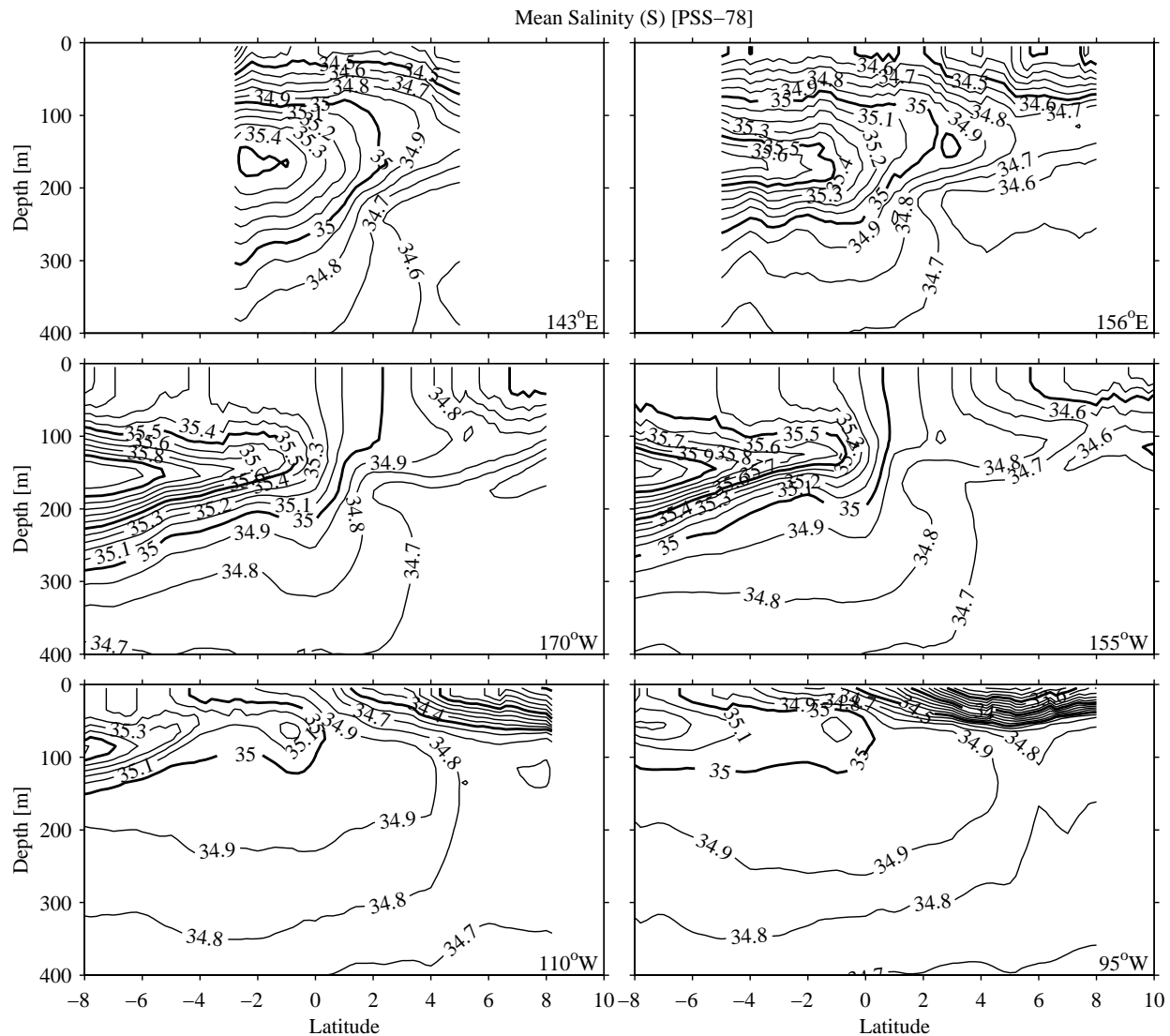


Fig. 4 (left). Sections of mean salinity (S) estimated at 10 nominal longitudes and along the equator, following Fig. 2. Contour interval is 0.1, with heavy contours at 0.5.

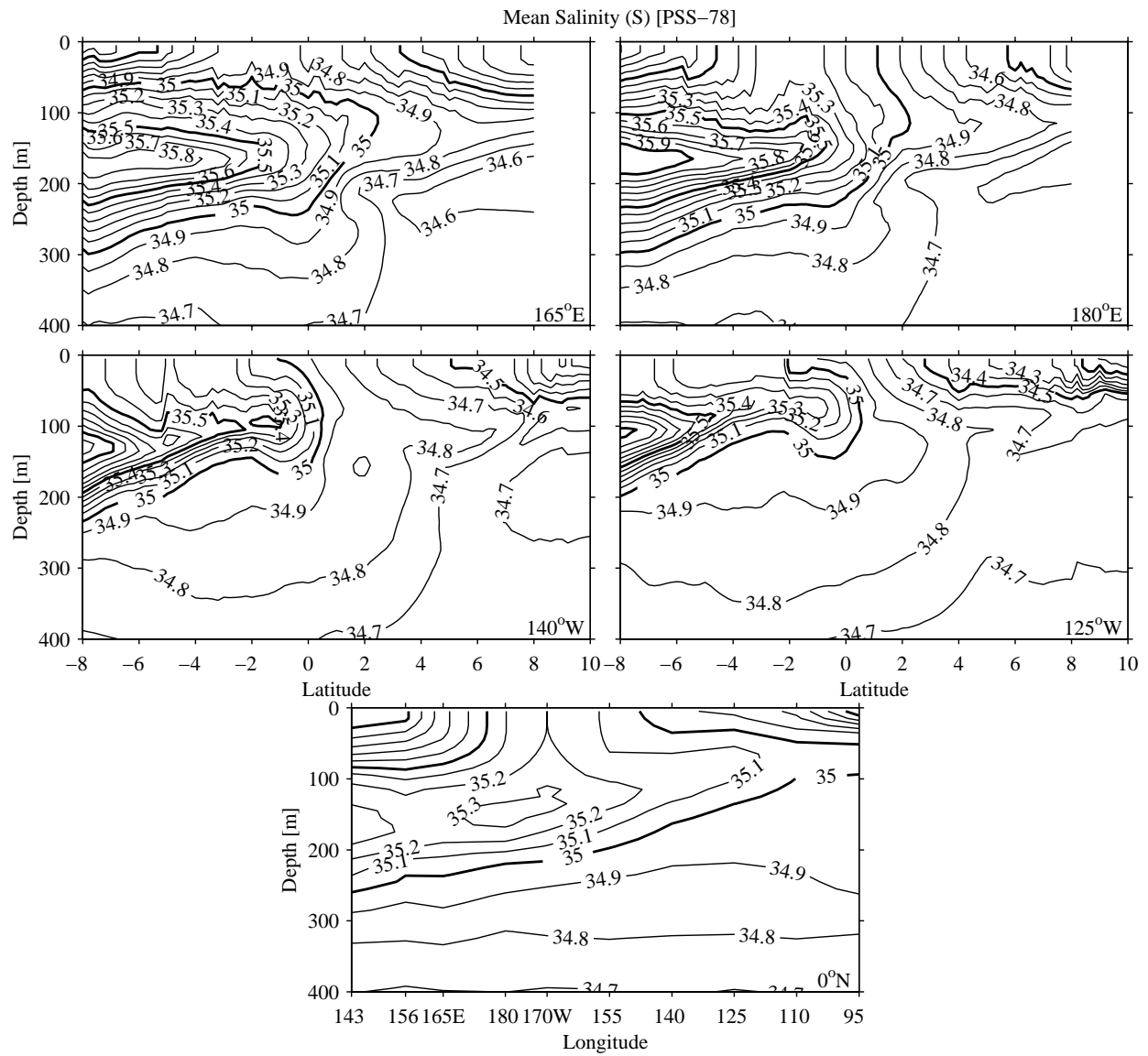


Fig. 4 (right).

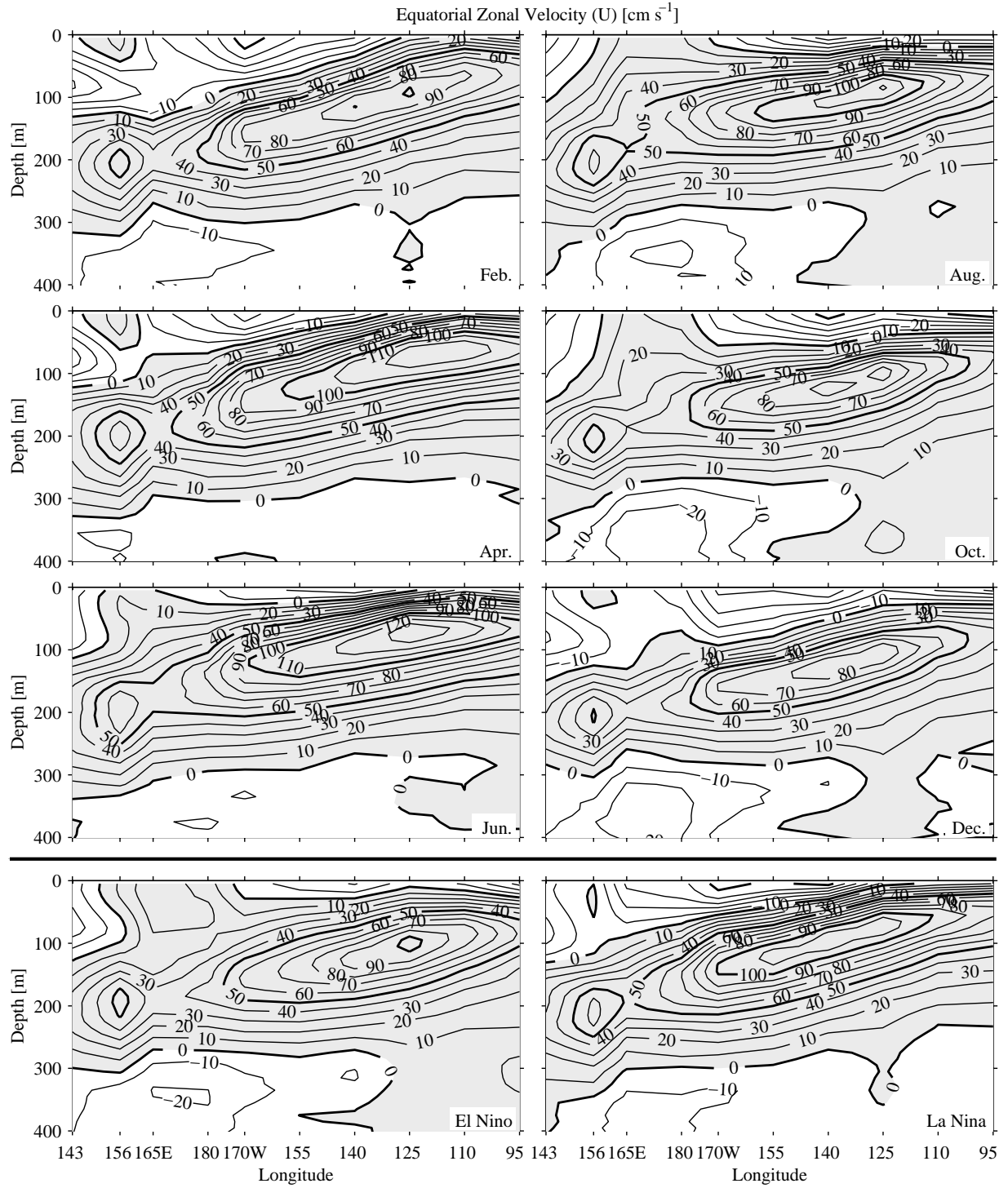


Fig. 5. Zonal sections of zonal velocity (u) along the equator estimated for 6 months and both phases of the ENSO cycle. Six months of a SOI = 0 (normal) year are shown in the upper six panels as described in the text. SOI = -1 (El Niño) is shown in the bottom left panel and SOI = +1 (La Niña) in the bottom right panel. Details follow Fig. 2.

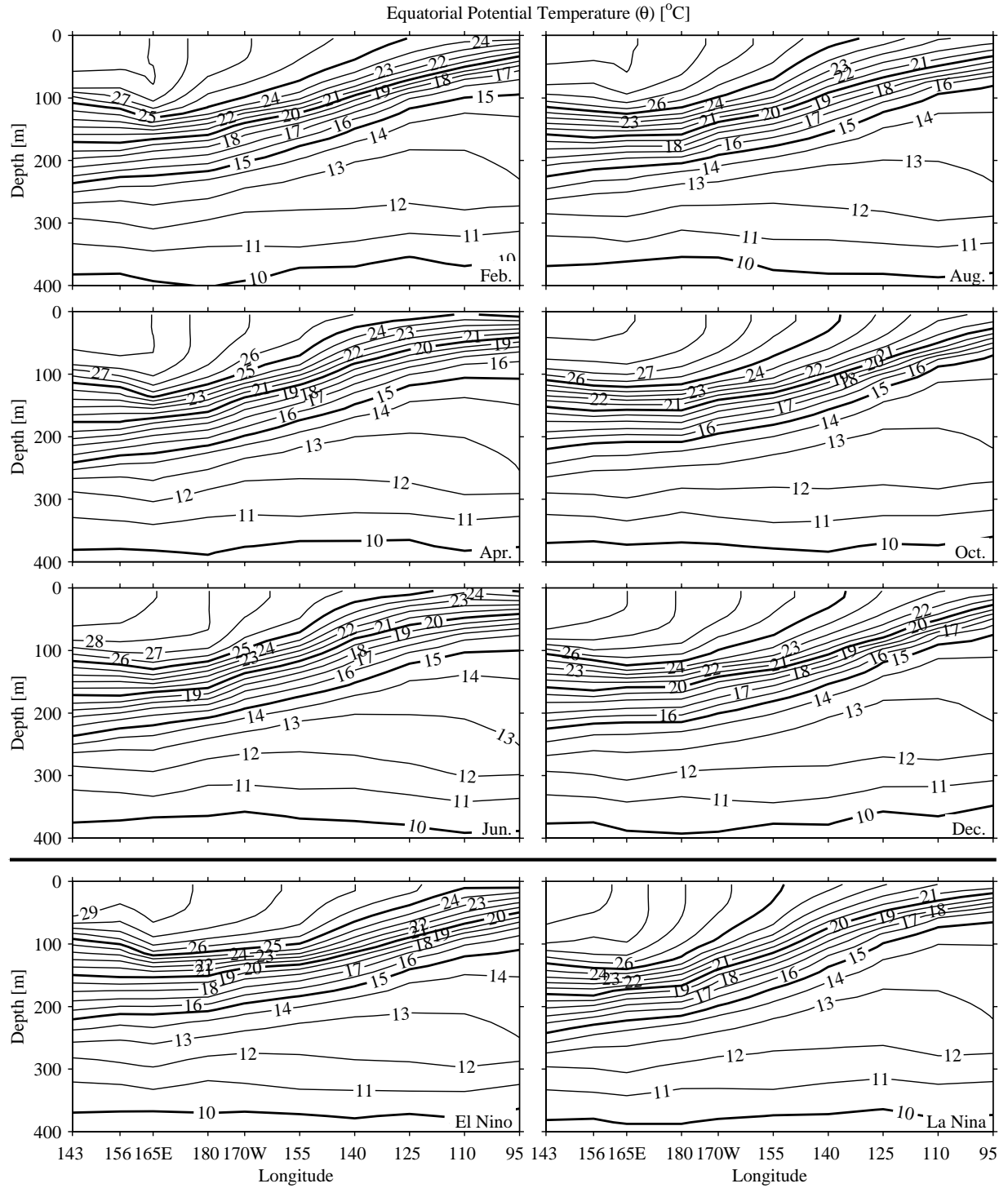


Fig. 6. Zonal sections of potential temperature (θ) along the equator estimated for 6 months and both phases of the ENSO cycle. Details follow Fig. 3.

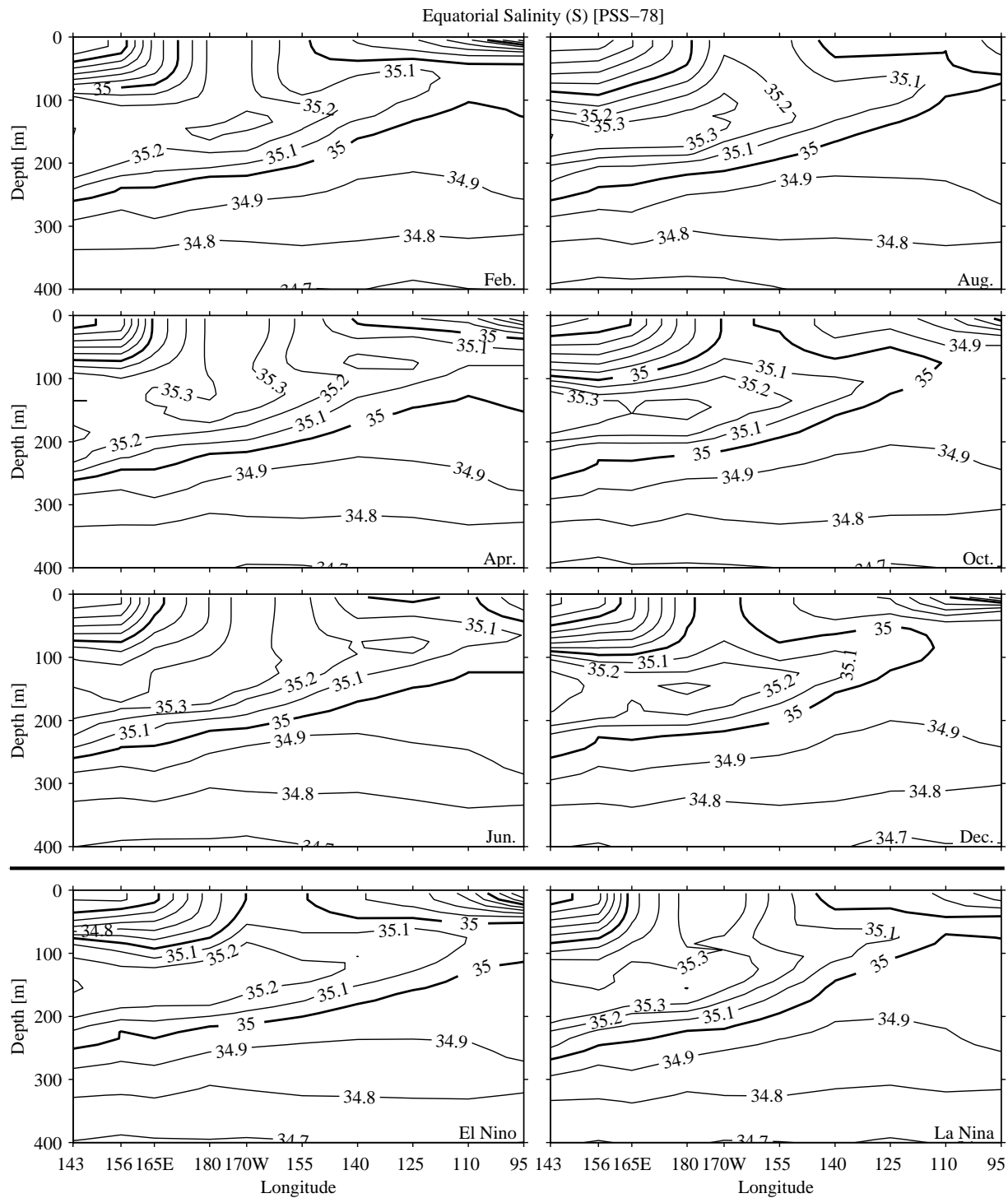


Fig. 7. Zonal sections of salinity (S) along the equator estimated for 6 months and both phases of the ENSO cycle. Details follow Fig. 4.

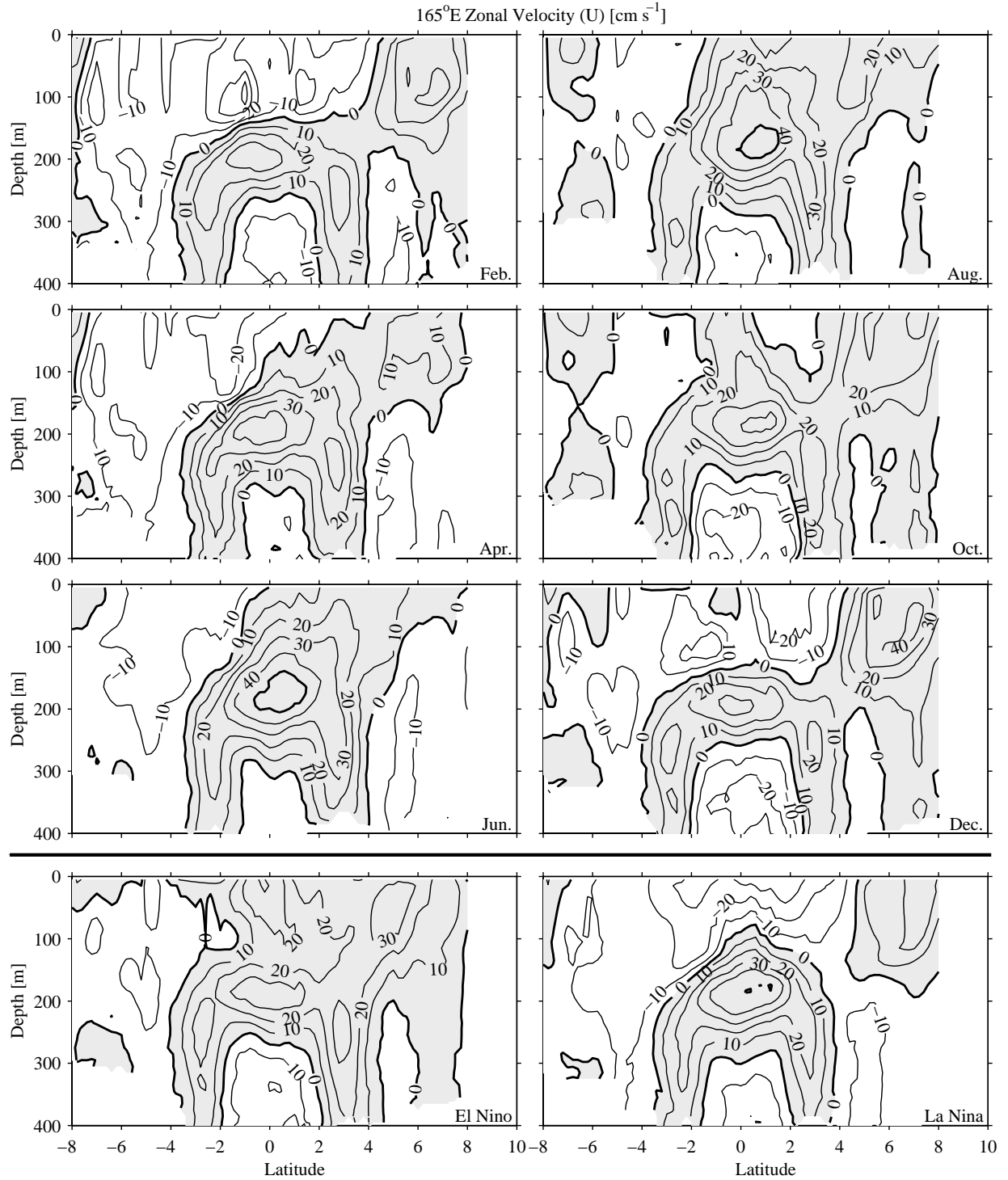


Fig. 8. Meridional sections of zonal velocity (u) at 165°E estimated for 6 months and both phases of the ENSO cycle. Details follow Fig. 2.

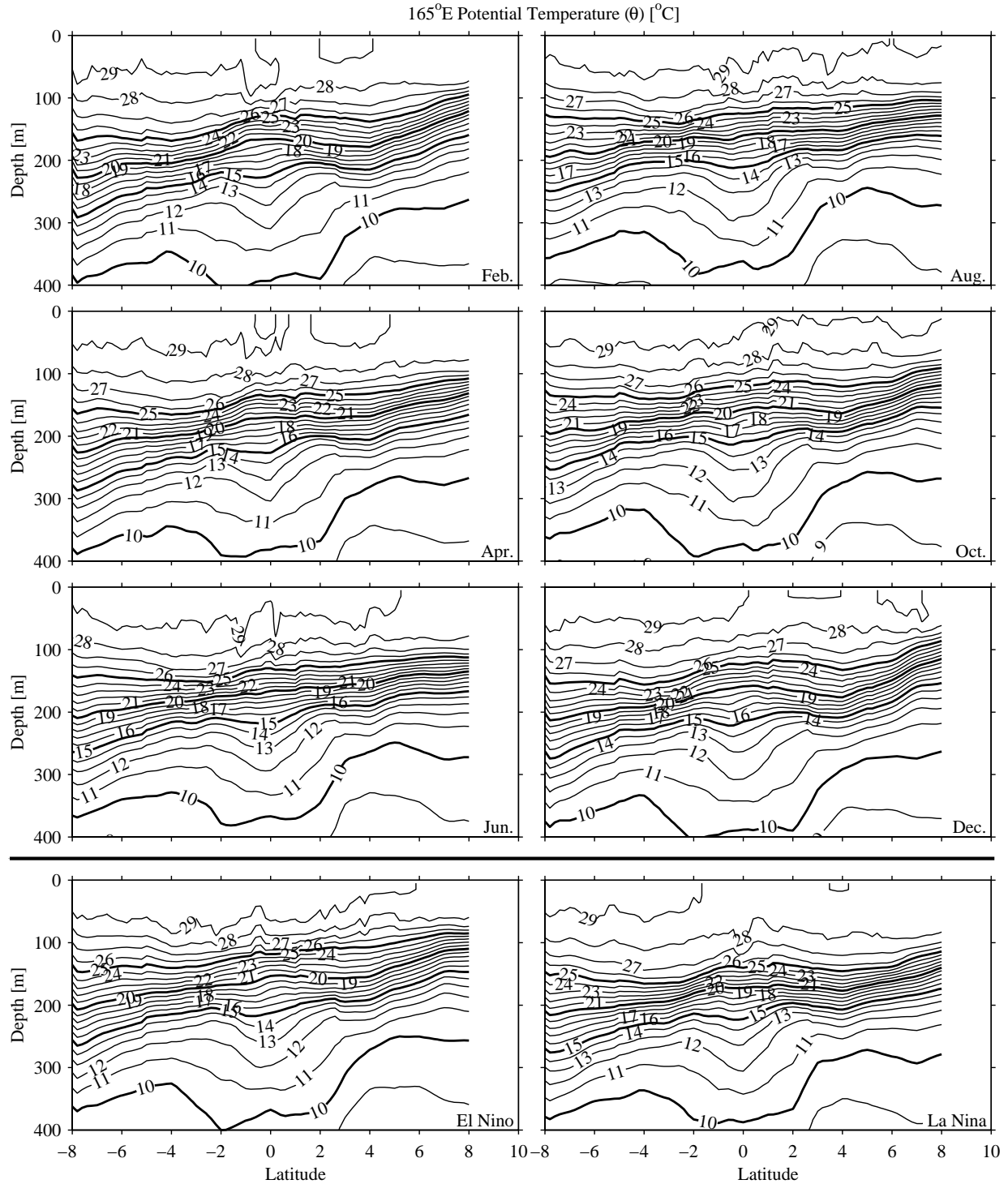


Fig. 9. Meridional sections of potential temperature (θ) at 165°E estimated for 6 months and both phases of the ENSO cycle. Details follow Fig. 3.

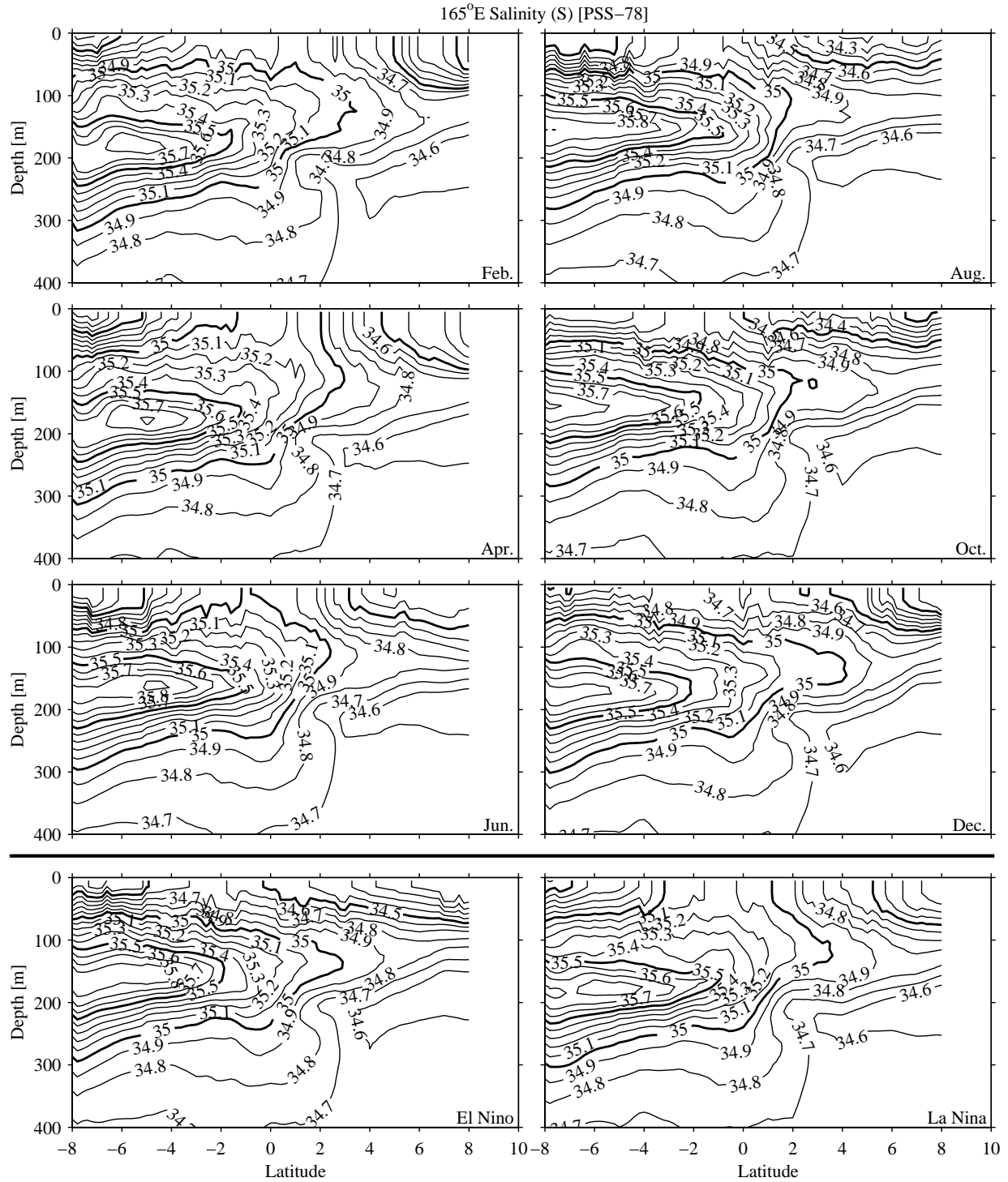


Fig. 10. Meridional sections of salinity (S) at 165°E estimated for 6 months and both phases of the ENSO cycle. Details follow Fig. 4.

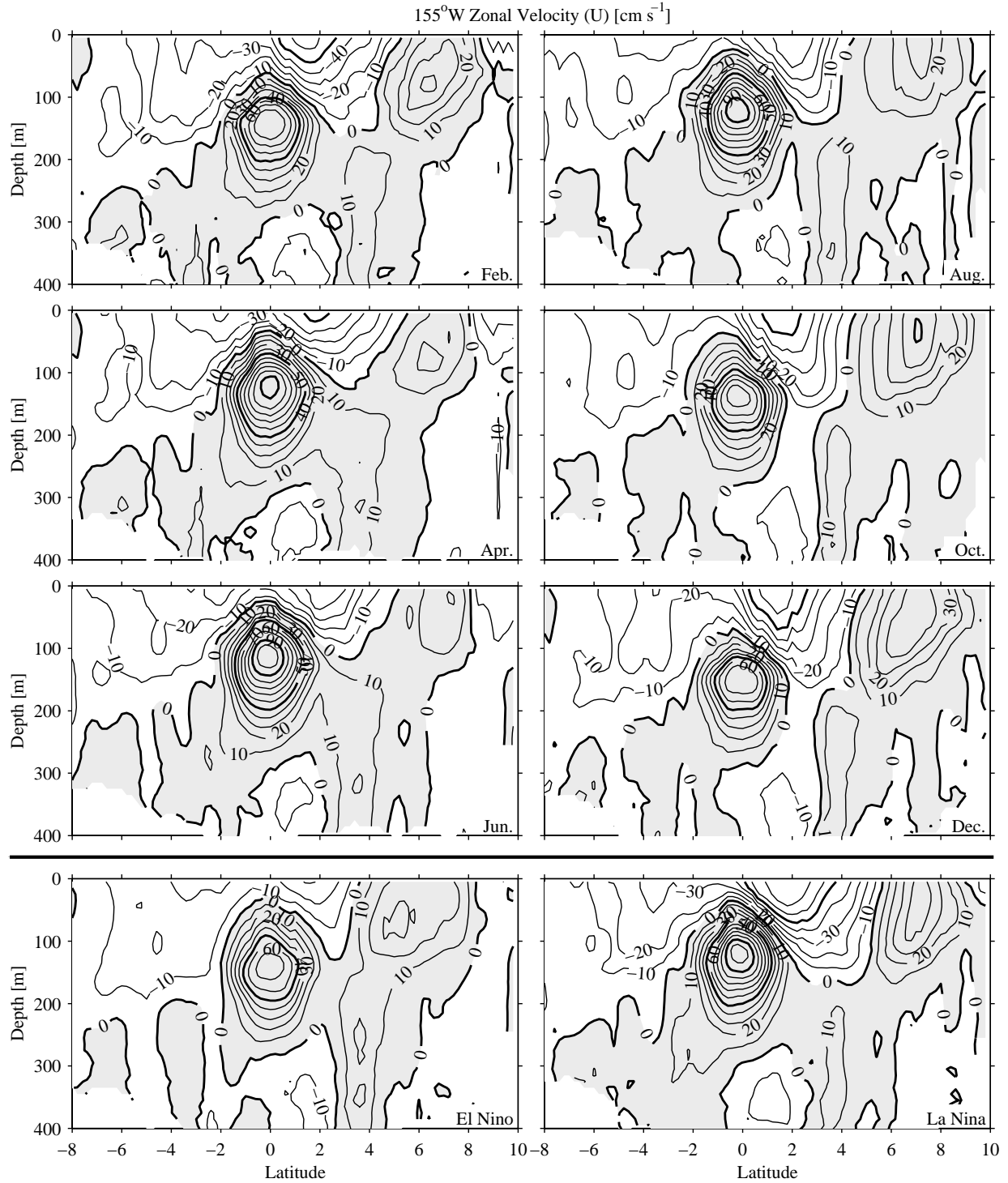


Fig. 11. Meridional sections of zonal velocity (u) at 155°W estimated for 6 months and both phases of the ENSO cycle. Details follow Fig. 2.

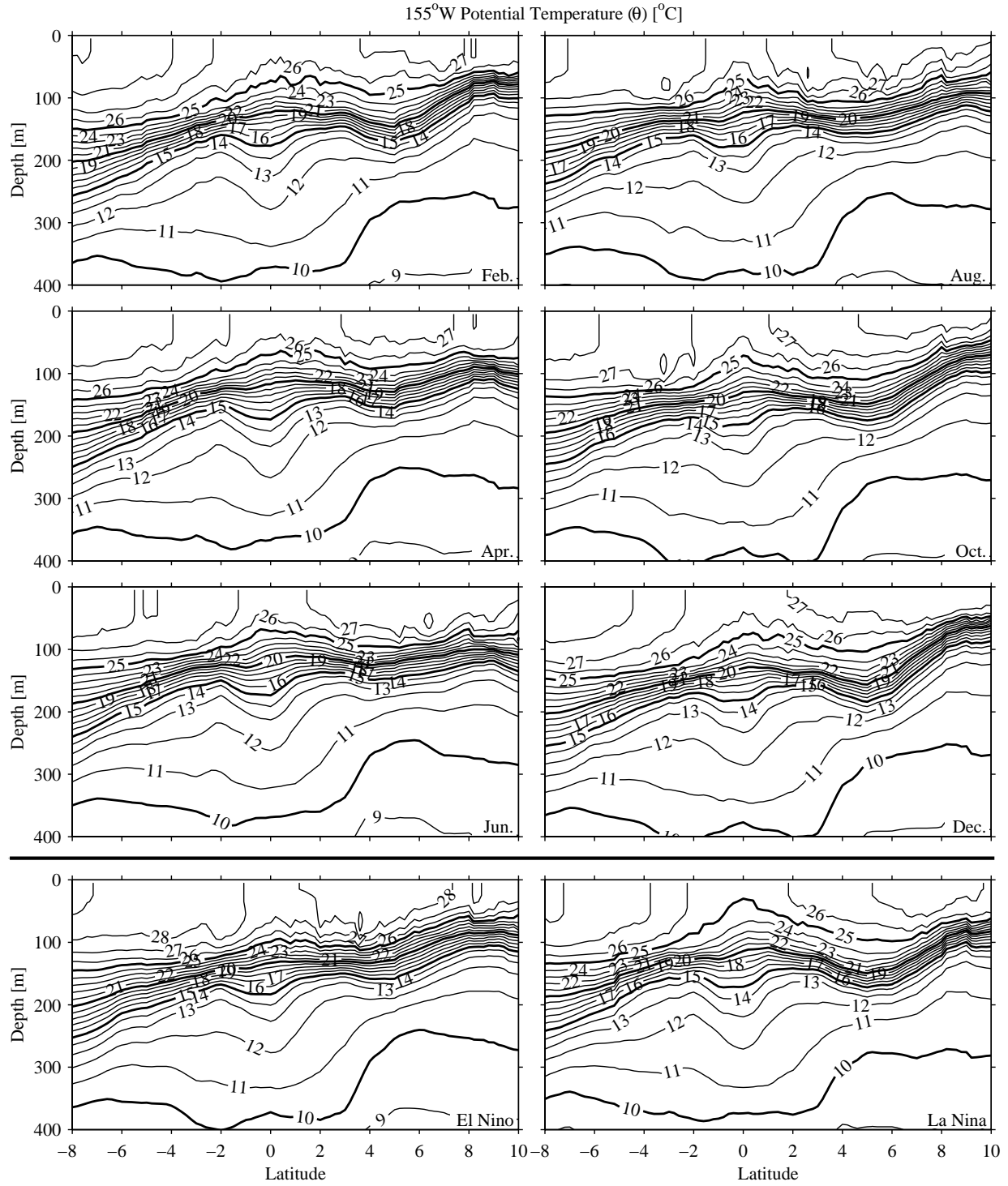


Fig. 12. Meridional sections of potential temperature (θ) at 155°W estimated for 6 months and both phases of the ENSO cycle. Details follow Fig. 3.

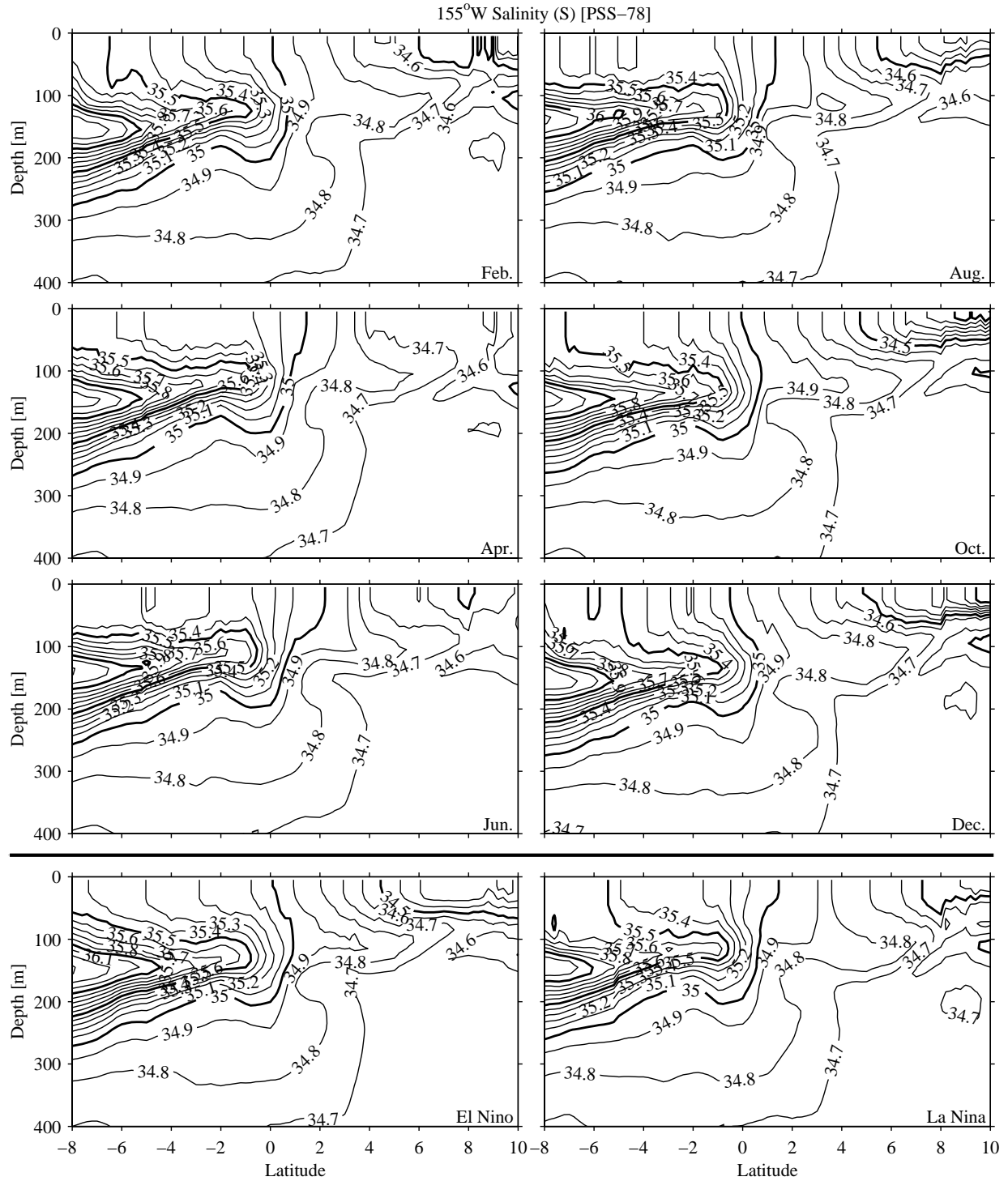


Fig. 13. Meridional sections of salinity (S) at 155°W estimated for 6 months and both phases of the ENSO cycle. Details follow Fig. 4.

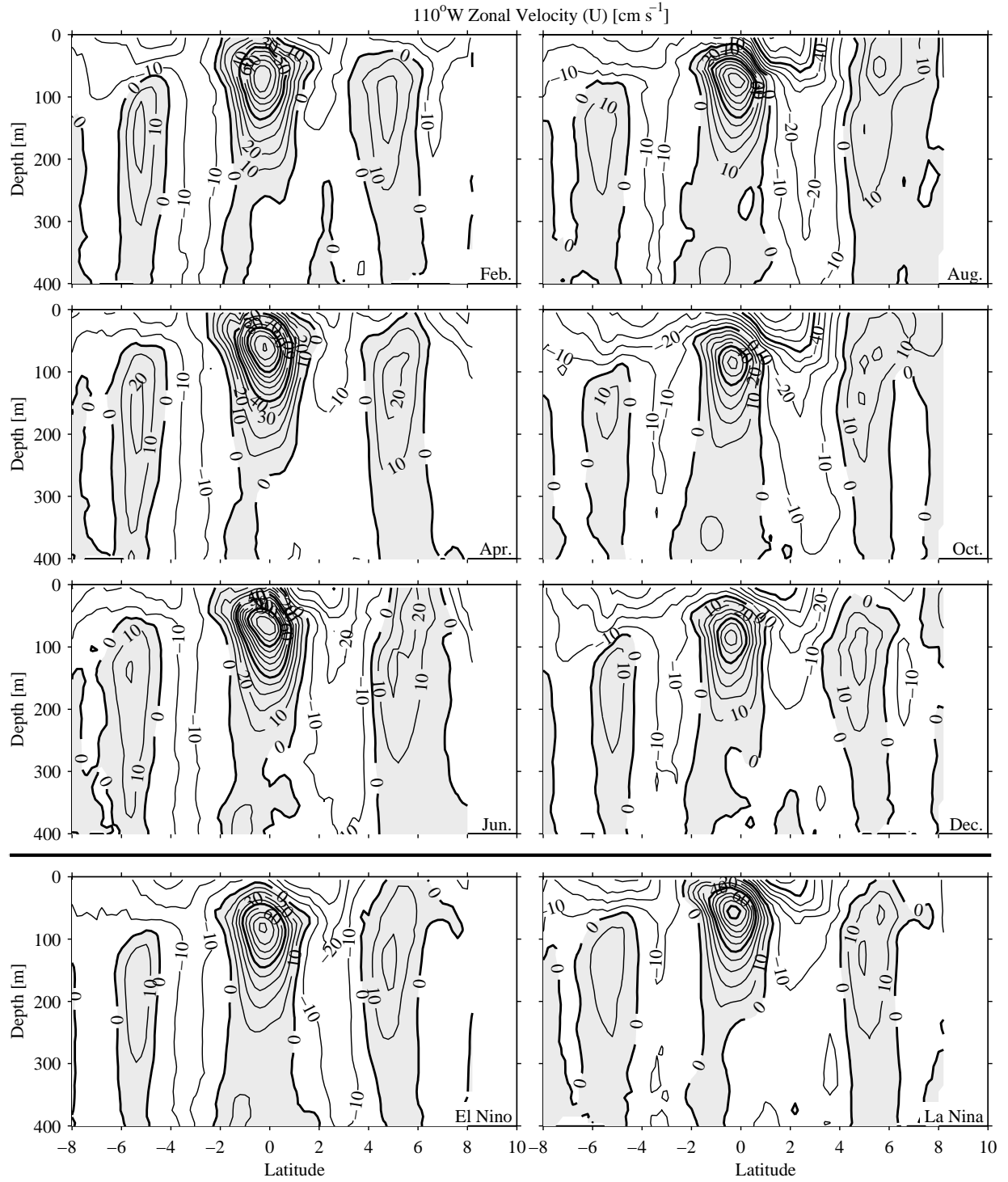


Fig. 14. Meridional sections of zonal velocity (u) at 110°W estimated for 6 months and both phases of the ENSO cycle. Details follow Fig. 2.

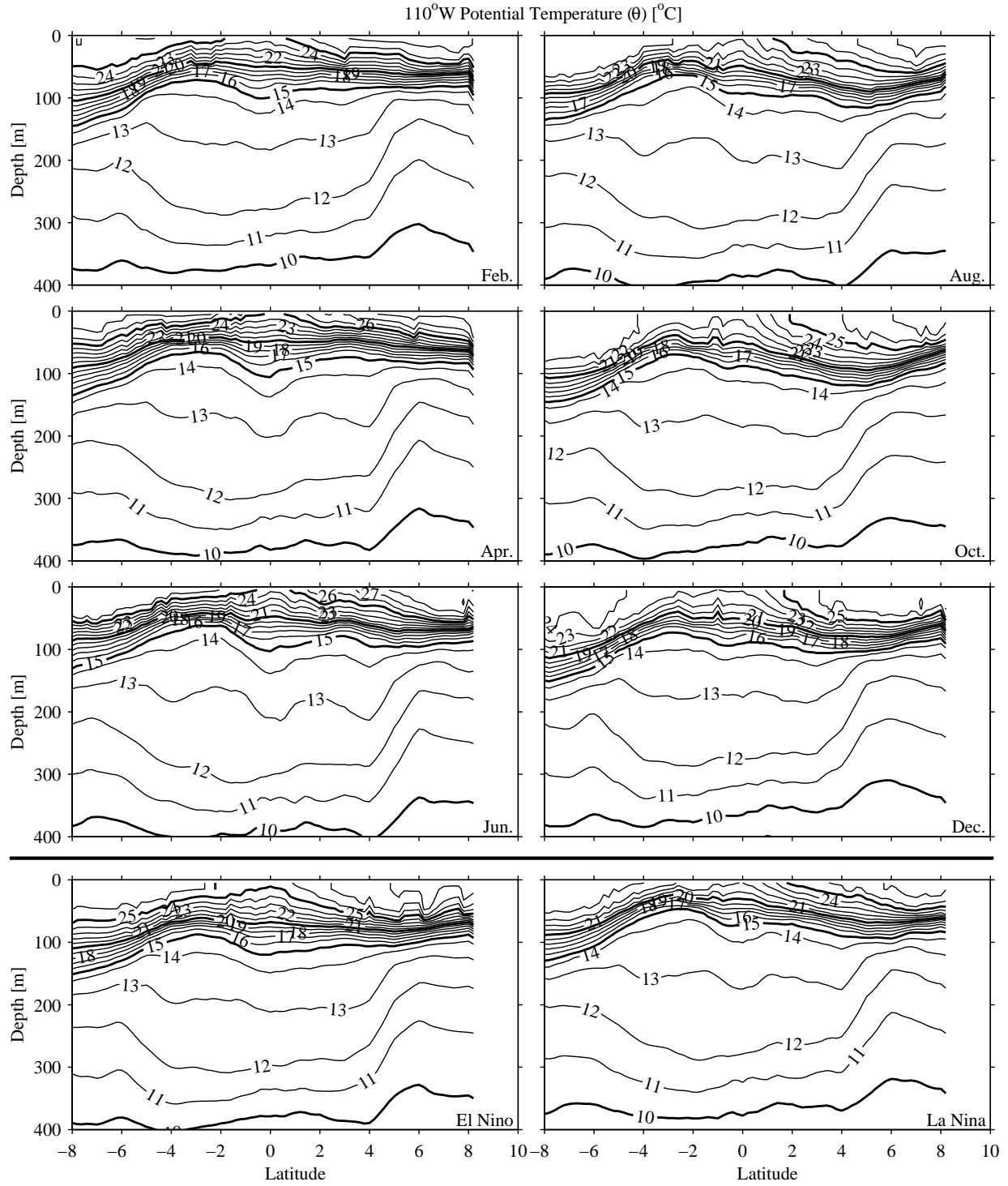


Fig. 15. Meridional sections of potential temperature (θ) at 110°W estimated for 6 months and both phases of the ENSO cycle. Details follow Fig. 3.

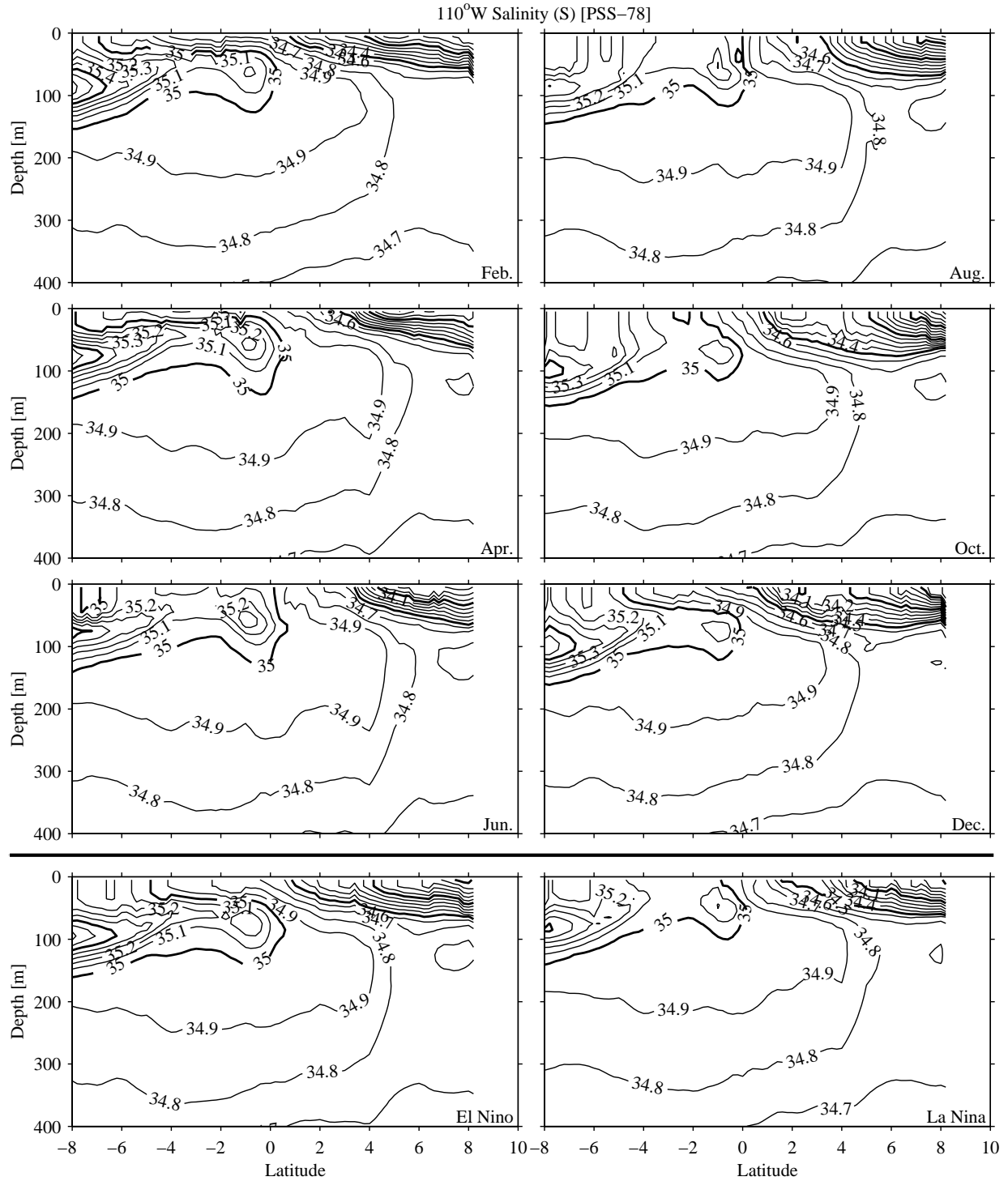


Fig. 16. Meridional sections of salinity (S) at 110°W estimated for 6 months and both phases of the ENSO cycle. Details follow Fig. 4.

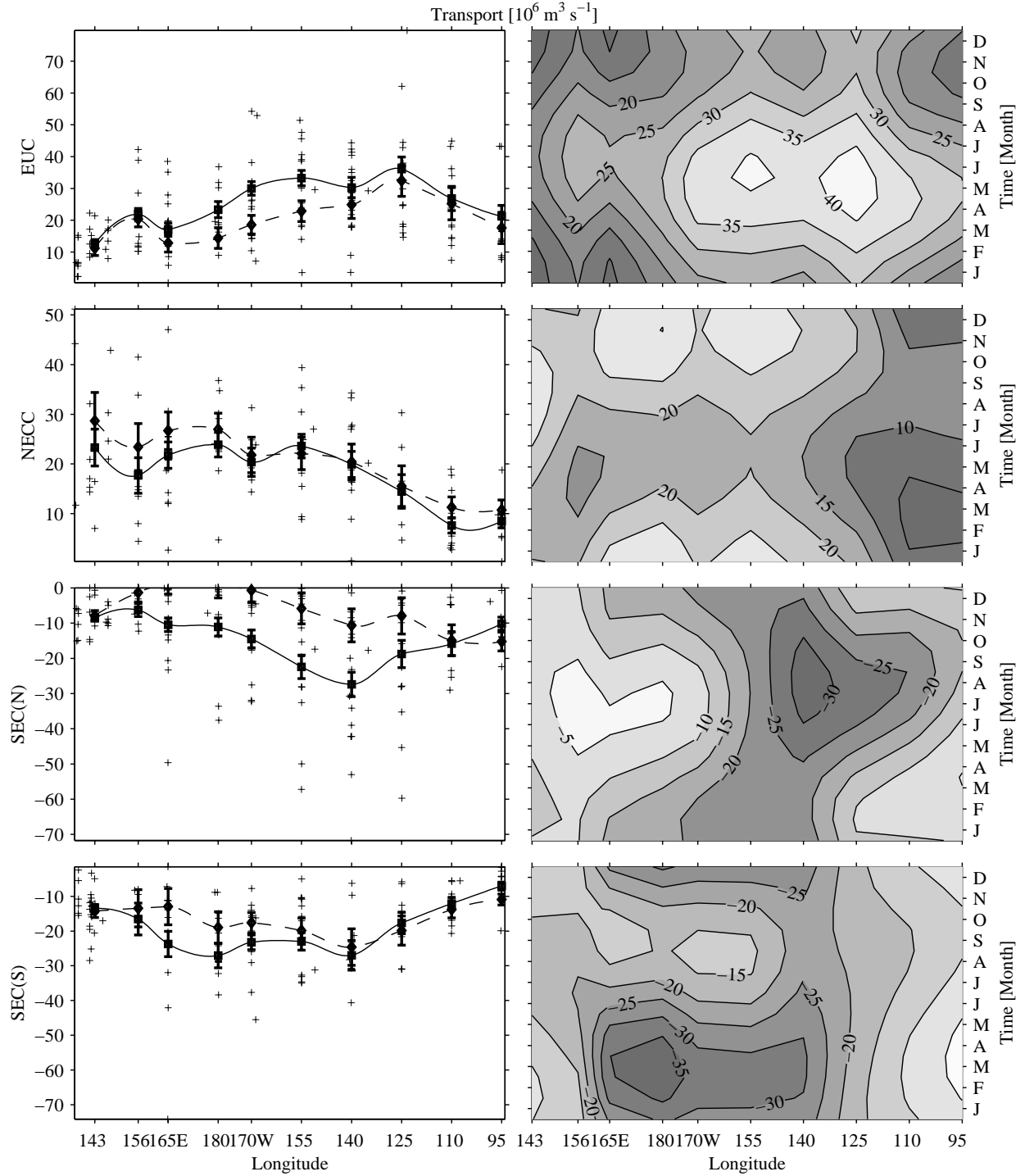


Fig. 17. Zonal current volume transport [$10^6 \text{ m}^3 \text{ s}^{-1}$] for (from top to bottom) the EUC, NECC, SEC(N), and SEC(S). Left panels show the quantity with error bars versus longitude for means (■'s joined by solid lines), SOI = -1.5 strong El Niño (◆'s joined by dashed lines), and raw data (+'s). Right panels show contours of the seasonal cycle versus longitude. Contour interval in the right panels is $5 \times 10^6 \text{ m}^3 \text{ s}^{-1}$ and the y-axis tick marks on the left panels are at twice that interval.

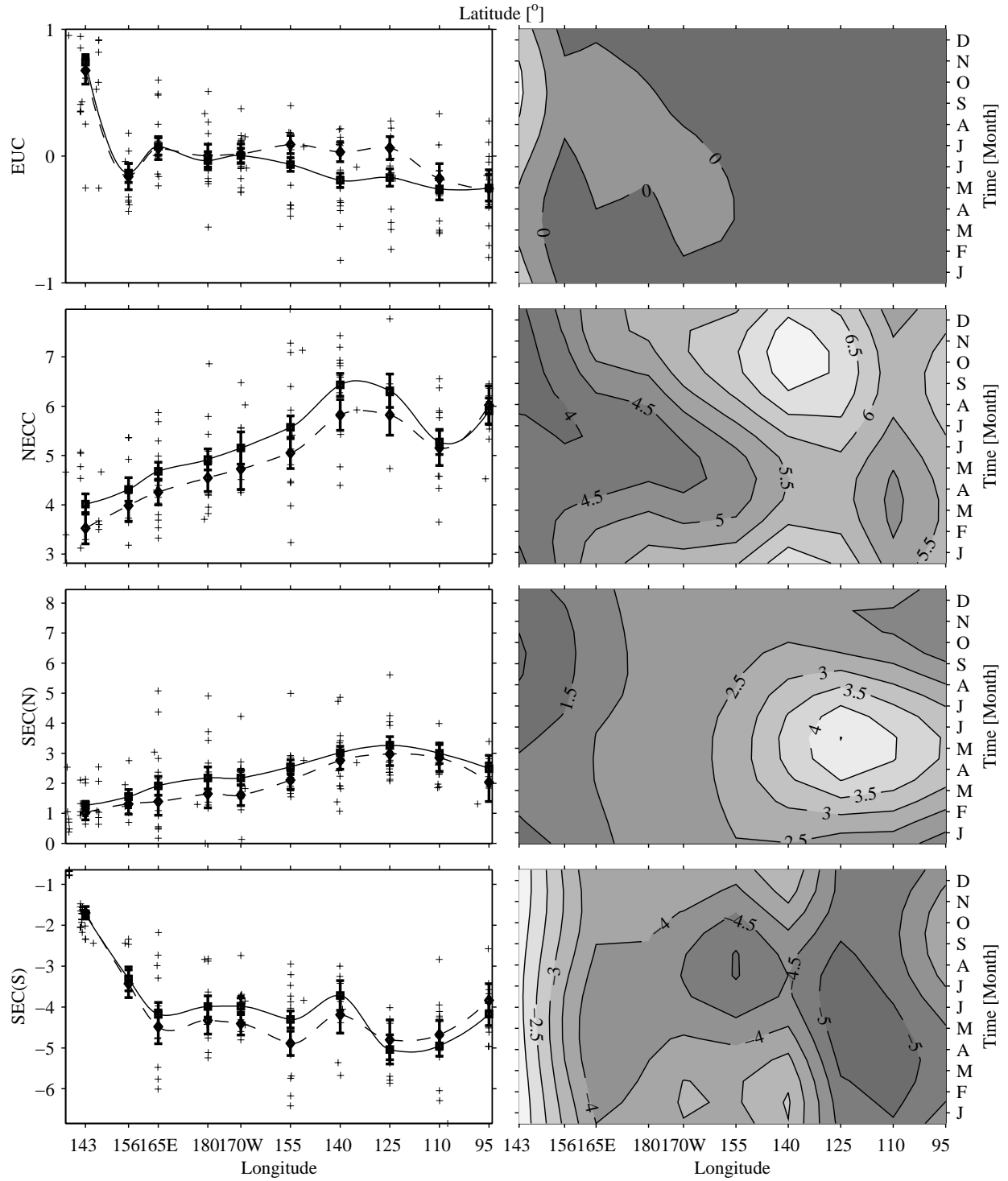


Fig. 18. Zonal velocity-weighted current latitude [°] for (from top to bottom) the EUC, NECC, SEC(N), and SEC(S). Contour interval in the right panels is 0.5° and the y-axis tick marks on the left panels are at twice that interval. Details follow Fig. 17.

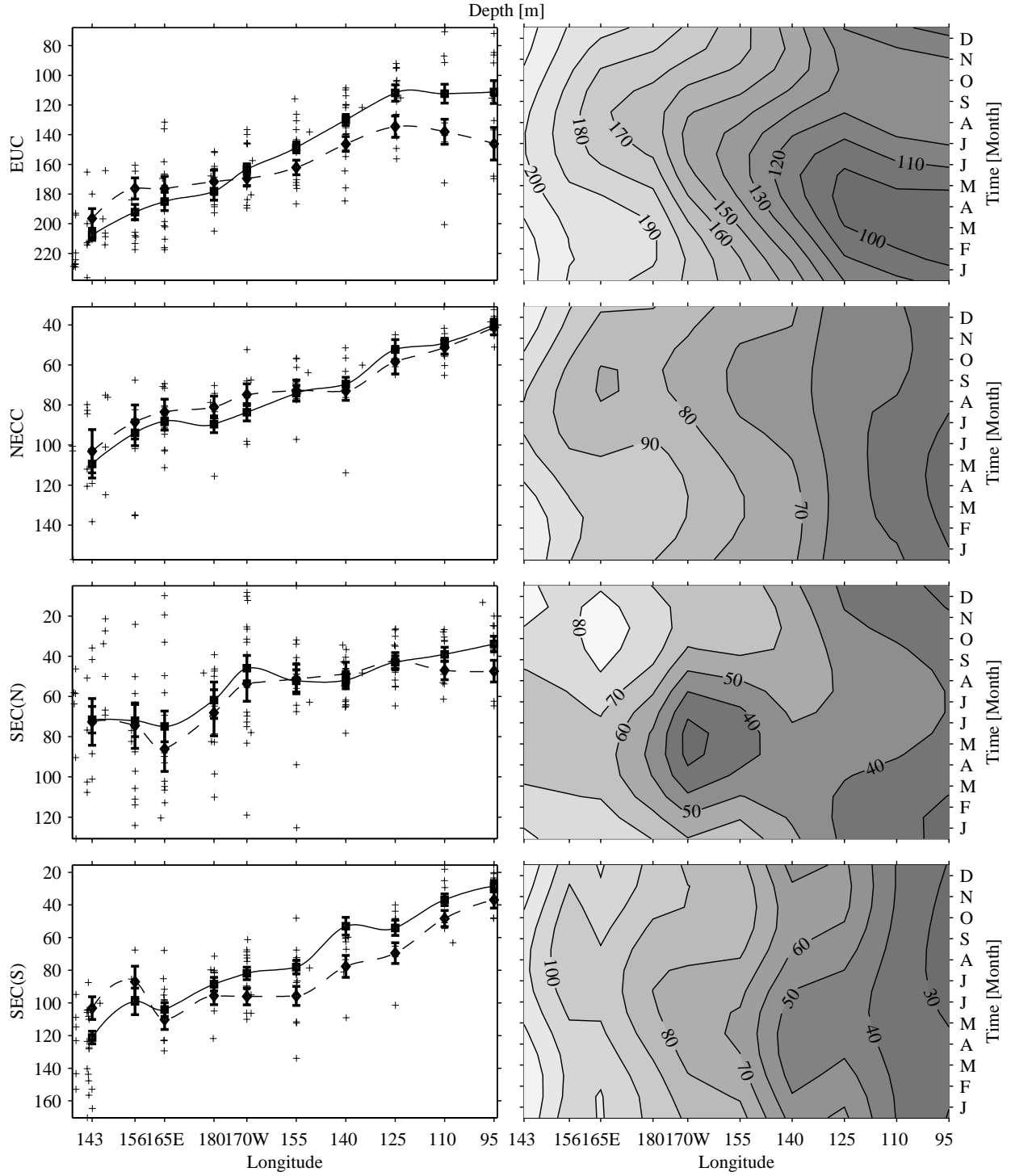


Fig. 19. Zonal velocity weighted current depth [m] for (from top to bottom) the EUC, NECC, SEC(N), and SEC(S). Contour interval is in the right panels is 10 m and the y-axis tick marks on the left panels are at twice that interval. Details follow Fig. 17.

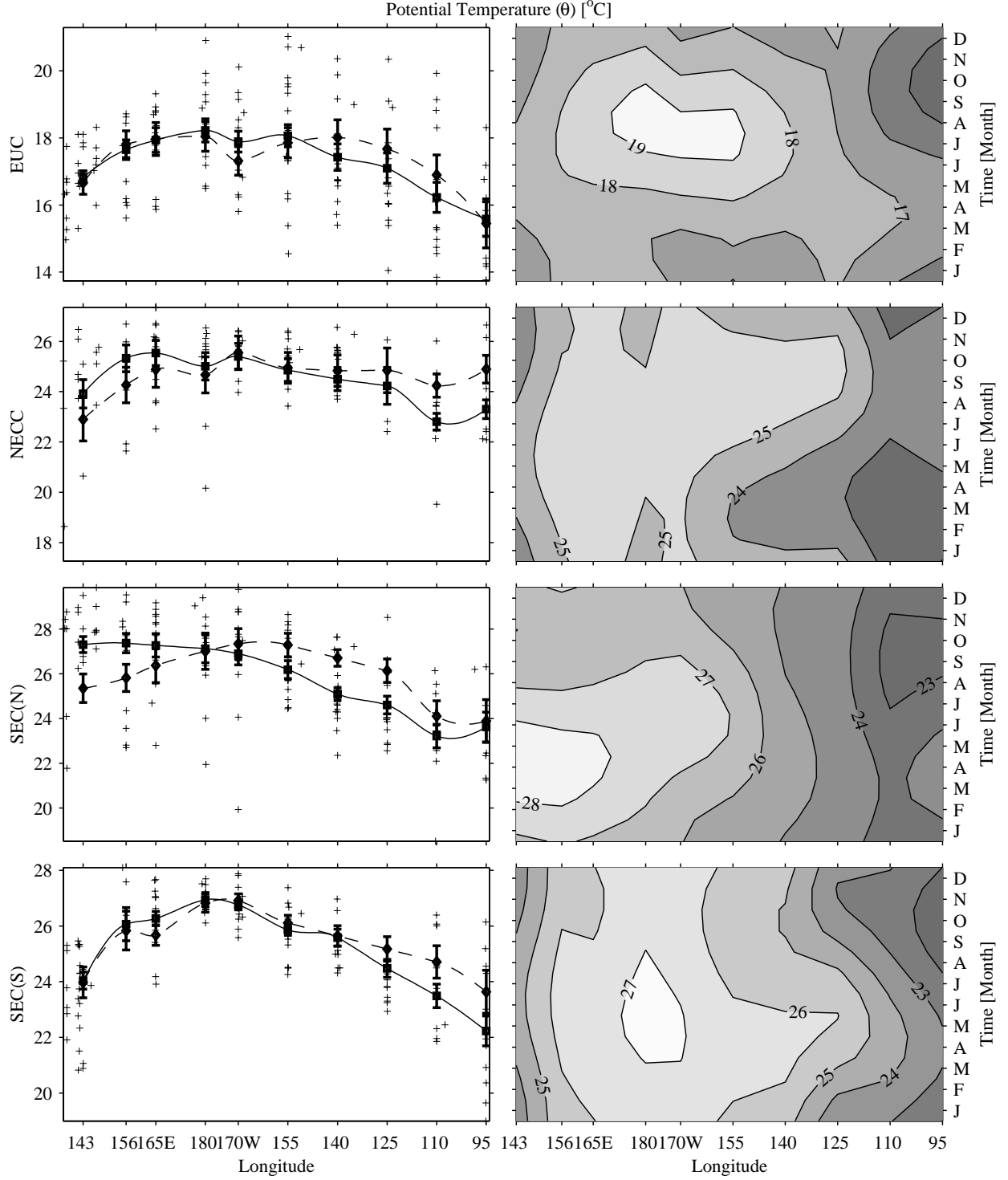


Fig. 20. Zonal velocity-weighted current temperature [$^{\circ}\text{C}$] for (from top to bottom) the EUC, NECC, SEC(N), and SEC(S). Contour interval in the right panels is 1 $^{\circ}\text{C}$ and the y-axis tick marks on the left panels are at twice that interval. Details follow Fig. 17.

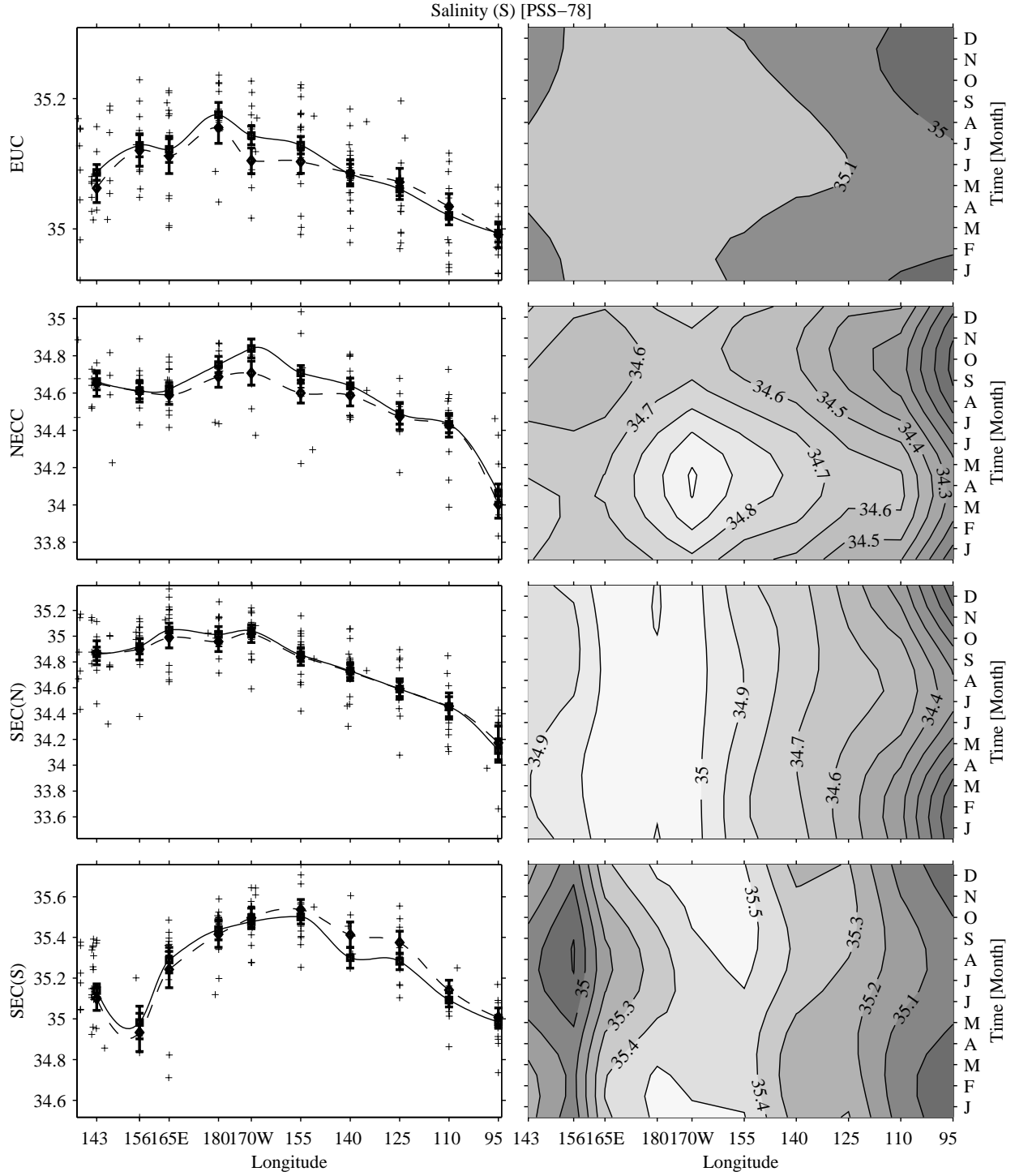


Fig. 21. Zonal velocity-weighted current salinity [PSS-78] for (from top to bottom) the EUC, NECC, SEC(N), and SEC(S). Contour interval in the right panels is 0.1 and the y-axis tick marks on the left panels are at twice that interval. Details follow Fig. 17.